Nonhydrostatic XBeach Simulation of Wave Transformations in a Fringing Reef Environment: Validation using Field Observations

A PLAN A THESIS SUBMITTED TO THE GRADUATE DIVISION OF THE UNIVERSITY OF HAWAIʻI IN PARTIAL FULFILLMENT OF THE REQUIREMENTS FOR THE DEGREE OF

MASTERS OF SCIENCE

IN

OCEAN AND RESOURCES ENGINEERING

AUGUST 2024

By
Charlotte E. White

Thesis Committee:

Z. Huang, Chairperson
K.F. Cheung
B.A. Jones

Acknowledgements

There are many people I'd like to thank for their support during this project. I wish to acknowledge my committee members Kwok Fai Cheung and Ben Jones for their continued support and knowledge during my studies. I am especially grateful to my advisor, Zhenhua Huang. His expertise and guidance were instrumental throughout my research. I am appreciative of Cary Troy for inspiring my interest in ocean engineering and of the ORE faculty for their dedication to teaching and mentorship. I'd also like to thank my ORE classmates, particularly Clint Reyes, Jonathan Chase and Shijie Huang. Your insight and guidance have helped me immeasurably.

I would also like to thank those at R3D who have made contributions to this research project, including Josh Levy, Ben Jones, Brady Halverson, Mert Gokdepe, Ian Robertson and Aryton Rodriguez. The collaboration towards the project and your support has been invaluable. Special thanks to Corey Olfe at the University of California San Diego for providing access to the PacIOOS wave buoy data. Your contribution was crucial for this research and your assistance is deeply appreciated.

Finally, I am deeply grateful to my friends for their constant encouragement and to my family for their unwavering support through this journey.

Abstract

Modeling wave transformations in nearshore fringing reef environments is an evolving field, especially for engineering applications. This study focuses on wave transformation at Waimānalo Beach, a location that features a shallow fringing reef and sloping seafloor. To study the wave characteristics at the site, the nonhydrostatic version of XBeach (nonhXB), a two-dimension, depth-integrated numerical model is implemented. The offshore boundary wave conditions are provided by the Simulating Waves Nearshore (SWAN) model. The bathymetry for the nonhXB model is prepared using US Army Corps of Engineers (USACE) 1-m resolution LiDAR data, while the bathymetry for the SWAN model is prepared with the NOAA 3-m resolution Continuously Updated Digital Elevation Model. This study adopts an approach by integrating in-situ field observations at Waimānalo Beach, as a method of calibrating the nonhXB model setup for the site. Waves at two nearshore locations were measured using pressure transducers. The results of the field survey reveal infragravity (IG) waves present at both pressure sensor locations. Using spectral input from a nearby offshore wave buoy, the ability of nonhXB to model IG waves was explored. It was found that the simulated results aligned reasonably well with those of the field observations, including IG waves. Finally, the study examined how bottom roughness affects the presence of the IG waves. It was concluded that increasing the bottom roughness decreases the magnitude of the IG waves, as well as the probability of waves breaking at the site.

Table of Contents

List of Tables

List of Figures

Chapter 1

Introduction

1.1 Motivation

In recent years, the Hawaiian Islands have experienced chronic coastal erosion, threatening infrastructure and ecosystems. The rising population in Hawai'i heightens the demand for solutions to this increasingly complex problem, particularly in the winter months (November-March). The winter season brings high wave energy, compared to the mild wave climate of the summer season. The high-energy wave environment causes the sand of a given beach to retreat offshore until the milder summer waves can return the sand to shore (Stopa et al. 2013). Hardening the shoreline using man-made structures causes disruptions in the sand budget along the coast, resulting in overall coastal erosion. A study by Fletcher et al. (2012) found that a total length of 8.7 km, or 8%, of the original sandy beach of Oahu was lost between 1928 and 2007, mainly caused by anthropological modifications. The same study found that the island of Oahu experiences a long-term average shoreline change of -0.06 ± 0.01 m/yr. As beach hardening and sea level rise continue, the rate of shoreline loss along some beaches will increase and may lead to total beach starvation (Fletcher et al. 2012).

One approach to mitigate the coastal erosion in Hawai'i aims to imitate a natural fringing reef by integrating traditional man-made structures with an environmentally friendly solution. Part of the Rapid Resilient Reefs for Coastal Defense (R3D) project, the hybrid structure is a submerged perforated breakwater that will both shield coastlines against erosion from large waves and runup and encourage marine life growth on the hybrid reef. As the structure is designed to attenuate the wave energy along the coast, the stability of the beach profile is anticipated to increase.

The location for the R3D project is Fort Hase Beach, situated on the eastern side of Oahu. It is on the southern tip of the Mōkapu Peninsula at the Marine Corps Base of Hawaiʻi (MCBH), meaning that military base access is required to visit the project site. Originally, the plan was to collect data at Fort Hase for validation of the numerical scheme to be used by XBeach simulations for scenario studies of wave transformation at the site. However, due to lack of accessibility at the base, the planned data collection could not be conducted at Fort Hase. As an alternative, Waimānalo Beach was selected a secondary location to collect data. This project site is a public beach and does not require base access. The assumption is that the numerical scheme that works for Waimānalo will also work for Fort Hase. The eastern coast of Oahu, including Fort Hase, features shallow fringing reefs and a gently sloping seafloor. Similarly, Waimānalo Beach is located on the same side of the island (see Figure 1.1). It features a gently sloping fore-reef with patches of sand that transitions into a steeper seaward back-reef. Despite its proximity to the Mōkapu Peninsula, Fort Hase experiences refraction of large Pacific swells from the north during the winter. Waimānalo Beach, due to its more southerly location, experiences less of the northerly swells and therefore a decreased chance of an inclement wave climate.

One concern with the R3D design is the stability of the structure and the hybrid reef that is attached to it. Breaking waves have the potential to damage both the submerged breakwater and the reef, as waves breaking cause high forces in the water column. An additional concern is the anchoring system for the structures. Extreme design conditions, caused by storm events, may increase wave energy at the site. Waves breaking on the anchoring system may impact their functionality and accelerate the corrosion process. Erosive and reflective properties of the infragravity wave components are also of concern. To ensure the structure remains intact and serves its intended purpose, it is crucial to study

Figure 1.1 Map of Oahu with Fort Hase and Waimānalo Project Sites Marked

the wave patterns presented at the project site. The transformation of wave energy in a nearshore environment can be studied using a nonhydrostatic depth-integrated model called XBeach (nonhXB). XBeach is an open-source numerical model that simulates hydrodynamic and morphodynamic processes at coasts.

1.2 Objectives

The main priority of this thesis is to utilize nonhXB to successfully study wave transformations over a fringing reef at the Waimānalo Beach site. One-way coupling between the nonhXB model and the SWAN model is implemented as the simulation method. To derive a numerical scheme suitable for the project site, several model parameters are tested within the nonhXB model. Intending to calibrate and validate the nonhXB results, another focus of this thesis is to conduct a field survey to collect in-situ wave data. The data is then analyzed and compared to the model results.

Furthermore, infragravity (IG) waves are a significant component of the nearshore environment and are a concern for the R3D project. As they were revealed in the field tests, the ability to simulate them in nonhXB is a key aspect of this project. One parameter known to impact the wave energy dissipation of IG waves, bottom roughness, is studied to better understand their influence within nonhXB simulations.

The fundamental hypotheses to be tested in this research are as follows:

1. The nonhXB model can be effectively implemented to study the wave transformations of a fringing reef.

2. The field data collected using pressure sensors can be used to calibrate and verify the nonhXB model results.

3. NonhXB is capable of simulating IG waves for the project location.

4. Bottom roughness has a significant impact on the simulation results, in particular, the IG waves.

The answer to the first hypothesis can be found by carrying out preliminary nonhXB simulations to optimize a feasible numerical scheme. The model should have a balance between the resolution, which affects accuracy, and computational expense. One aspect of the nonhXB model that impacts the computational time is the number of layers that the vertical component, or water column, is divided into. The most common two divisions are the single layer and reduced two layer models, whose applicability are studied for this project site (de Ridder et al. 2021). An additional parameter that impacts the wave transformations is the bottom roughness (Nielsen 1992). A preliminary investigation of bottom roughness in the nonhXB model is conducted to better understand its effects.

To test the second hypothesis, a preliminary field survey took place at Waimānalo Beach. Waves were measured at two nearshore locations using pressure transducers. The results from the field survey can be compared to the nonhXB model outputs to calibrate and validate the model. The data collected can also be analyzed for IG waves, which addresses the third hypothesis. The ability of nonhXB to simulate IG is tested using wave buoy spectral input from the day of the field survey as the input spectrum. Finally, the fourth hypothesis is focused on understanding how bottom roughness impacts the wave transformations. By investigating different bottom roughness values, the change in wave conditions can be studied, especially the influence on IG waves. Overall, this thesis aims to validate the nonhXB numerical schemes for a reef environment using field observations and to understand the significant factors influencing wave transformations, particularly the role of bottom roughness on IG waves.

1.3 Literature Review

XBeach was originally formulated to model hydrodynamic and morphodynamic processes of a plane beach using a 1D approximation. Beginning a phase-averaged, depth-integrated hydrodynamic model, XBeach was the framework to assess hurricane impacts on the United States coasts (McCall et al. 2022). It has since advanced to include depth integration and is now capable of modeling both hydrostatic and nonhydrostatic simulations. The ability to simulate nearshore processes has allowed the numerical model to be applied to nearshore fringing reef environments, though requiring some adjustments to accurately represent the reef components (Lashley et al. 2018; Sheremet et al. 2011). Nonhydrostatic models are being increasingly implemented because of their capabilities for their scalability, accessibility and nonlinear wave characteristics (Bai and Cheung 2016).

As phase-resolving models use governing conservation equations to describe individual wave transformations, each simulation is a high computational expense and limits the area to be simulated (Lashley et al. 2018; Buckley et al. 2014). For this reason, it is common to transition from a phase-averaged model into a phase-resolving model to maintain the individual wave transformations nearshore but allow for a larger study area (Cheung et al. 2003). Simulating Waves Nearshore (SWAN) model, which is a common phase-averaged model, is often used in conjunction with nonhXB for this purpose. SWAN is able to produce the wave energy spectrum for a large domain over long durations, which helps handle the transformation between deep and coastal water for nonhXB (Booij et al. 1999). A study conducted by Selman (2023) explored the ability of nonhXB to reproduce the SWAN spectral input. The results found that nonhXB was in poor agreement with the SWAN input for steep wave conditions due to super-harmonic components. The model linkage was successful for calmer wave conditions (Selman 2023).

Beyond the size of the domain, the resolution is also a limiting factor. As the phase-resolving model formulation solves the individual wave transformations, it is capable of capturing wave movements within a wavelength. Increasing the resolution of the domain's grid increases the computation expense, therefore a balance must be found (de Ridder et al. 2021). Several studies investigated the optimal resolution within reasonable computational resources. Research done by Jacobs (2010) found that 30 grid points per wavelength is sufficient to capture the wave characteristic in a nearshore environment. Using this study as a baseline, a thesis written by Chase (2023) found that 70 grid points per wavelength was a preferable resolution, despite increased computation time. The research done by Selman

(2023) also found that increased grid resolution provided an improved result concerning wave steepness.

An additional aspect of the model is the number of vertical computational layers of the water column. Increasing the number of layers has been shown to improve the dispersive properties in nonhydrostatic models without the need to increase the order of the spatial derivatives (Stelling and Zijlema 2003b). Additional layers cause significantly higher computational costs as a result of the increased matrix system, as the matrix grid points multiply per the number of layers employed (Jacobs 2010). A study conducted by Smit (2008) concluded that a two layer numerical scheme increased computational time significantly while only improving the results slightly, suggesting a single layer model for efficiency and better balance. To improve the imbalance in the computational expenses and maintain the dispersive properties of the original two layer model, the reduced version of the two layer model was introduced. It is reduced by simplifying the representation of the nonhydrostatic pressure, assuming that the nonhydrostatic pressure is constant in the lower layer. Several studies have concluded that the reduced two layer model is adequately capable of representing dispersion, while reducing computational time (de Ridder et al. 2021; Bai and Cheung 2016).

To calibrate nonhydrostatic model for a given location and assess the validity of the results, in-situ field observations and physical model experiments are often used as a comparison. A field study conducted on the coast of the United Kingdom deployed pressure transducers at four locations along a gravel beach to study the hydrodynamics and hydrology of storms. Its primary aim was to compare the collected data to a one layer, nonhydrostatic XBeach-G, which was developed to simulate storm impacts on gravel beaches. The results found that the model was able to predict wave transformations rather accurately for gravel beaches (McCall et al. 2014). In terms of model experiments, Chase (2023) conducted a large-scale wave flume experiment to validate the nonhXB numerical scheme implemented in his research. The conclusion of the research found that while the nonhXB simulations provided a reasonable agreement with the data collected during the wave flume experiment, it is unclear whether it can be adapted to real-world applications. Jacobs (2010) studied the nonhXB capabilities in a nearshore laboratory environment and concludes the study by recommending a real-world investigation of the nonhXB model.

One wave component IG waves, whose frequency is 0.004-0.04 Hz, are often researched in nearshore environments due to their strong impact on erosion, cross-shore sediment transport and reflective properties. IG waves are generated by several processes, including wave breaking and nonlinear wave interactions (Bertin et al. 2018). Edge waves are a type of infragravity waves that become trapped to the coast and travels along the shore. There are two main causes for edge waves. The first is due an oblique incident wave. Waves approach the coast at an angle refract and reflect, resulting in the wave being trapped. The second cause is due to resonance, which is influenced by the bathymetry of the wave environment. This can occur in enclosed or partially-enclosed basins, such as Waimānalo Bay. If the dimensions of the basin are such that the natural period of oscillation matches the period of incoming waves, resonance can amplify the edge wave. Water depth also plays a role in determining the resonant frequencies, as wave speed decreases in shallow water (Johnson 2007; Huntley and Bowen 1973).

The ability to model IG waves using nonhXB has been studied in both a laboratory fringing reef and real-world locations (Buckley et al. 2014; van Dongeren et al. 2012; Sheremet et al. 2011). Buckley et al. (2014) linked SWAN and nonhXB to predict the outcome of a laboratory steep fringing reef test. The results showed that the model was able to accurately capture gravity and IG wave height variation with reasonable accuracy. A field study at Ningaloo Reef in Australia was used as calibration for a nonhXB model to observe the transformation of IG waves over the reef. It was found that the two were in relatively good accordance and that bottom roughness played a large factor in wave energy dissipation rates (van Dongeren et al. 2012).

Bottom roughness is often cited as one of the main components of wave energy dissipation (Nielsen 1992; van Dongeren et al. 2012; Lowe et al. 2005; Buckley et al. 2016). Bretschneider et al. (1986) suggested a Manning coefficient of n = 0.035 for modeling roughness associated with the nearshore reefs and volcanic substrates, however the Mannings equation is an empirical equation that applies to uniform flow in open channels. The coastal environment with fringing reef introduces non-uniform flow. To accurately model flow resistance in coastal environments, it's often necessary to increase the Manning coefficient. This adjustment helps to account for the additional energy dissipation caused by the complex flow conditions and the presence of roughness elements (Lowe et al. 2005).

Moreover, the wave energy dissipated by bottom friction is greater in lower frequency waves than higher frequency waves. A study conducted at Kāneʻohe Bay, a site with fringing reef located between Fort Hase Beach and Waimānalo Beach, found that the two main components in the incident wave energy was dissipated by bottom friction and wave breaking. The incident wave energy was separated into short wave and IG wave components. While the short wave energy was mostly dissipated by wave breaking, the bottom roughness was found to have a higher impact on the IG waves. An additional finding of the study was that the use of a single hydraulic roughness along different frequency components can accurately describe the wave energy dissipation (Lowe et al. 2005). Another study investigated how varying bottom roughness impacted runup and setup due to IG waves in both a laboratory and SWASH model setting, finding that the greatest runup reduction was due to high bottom roughness in laboratory and simulated results (Buckley et al. 2022). Though the influence of bottom roughness is well studied, the extent of the literature does not present how different bottom roughness values influence the presence of IG waves in nonhXB results.

1.4 Project Scope

The primary goal of this thesis is to evaluate the performance of the nonhydrostatic XBeach model in simulating wave transformations at the Waimānalo Beach project site. The one and reduced two layer formulations of the model are compared to determine which option is more suitable for this research. The selected formulation can then be implemented to simulate the wave climate. To validate and calibrate the results of the nonhXB model, they are compared to field measurements. Using spectral input from a nearby wave buoy, the nonhXB model is used to analyze how bottom roughness influences IG waves and wave breaking probability. By calibrating the type of model and the bottom roughness, this research aims to provide a comprehensive comparison of the model and field observations, specifically gaining insights into the effects of bottom roughness on IG waves.

The parameters breaker steepness and reform steepness to define the wave breaking in nonhXB are of significance, however are out of the scope of this research project. The default breaker model is implemented. Furthermore, the grid used for this study was suggested by previous research. It is assumed the sensitivity of the grid is able to capture sufficient detail. Finally, the effects of the domain size of the simulations are not studied in this project.

1.5 Thesis Outline

The thesis is comprised of 5 chapters, as follows. Chapter 1 includes the project background, objectives and a literature review. Chapter 2 will consist of an overview of the methodology to achieve the objectives. This section will focus on the nonhydrostatic XBeach model, Simulating Waves Nearshore (SWAN) wave model, data required for the models and how the field observations will be made. Chapter 3 will then present the field observations made at Waimānalo Beach. Chapter 4 will discuss the parameters studied to properly calibrate the XBeach simulations, as well as make a comparison between the field observations and the nonhXB simulations. The final chapter, Chapter 5, will be a conclusion of the research and recommendations for future projects.

Chapter 2

Methodology

2.1 Introduction

This research employs the nonhXB model, an open-source software, for simulating coastal processes. The model operates in a depth-integrated, two-dimensional mode. XBeach's versatility in handling variable wave conditions and cost-effectiveness makes it suitable for this project. The model's complexity necessitates careful selection of methodology and comparison with field observations. The study also incorporates the Simulating Waves Nearshore (SWAN) model to address deep water statistics. The resolution and orientation of the numerical grids are critical considerations for accurate simulations. Field observations at Waimānalo Beach aim to validate the numerical scheme with the use of pressure transducers. This comprehensive approach integrates numerical modeling and field observations to enhance the understanding of wave transformations in complex coastal settings, contributing valuable insights to coastal engineering practices.

2.2 Data

The wave climate at the project site must be characterized to simulate the wave transformations into shore. The project had access to an Acoustic Doppler Current Profiler (ADCP), which would have been optimal to study the wave conditions specific to the project site, however the deployment timeline did not line up with this study. The two other sources that could have wave climate information on the project site would be a wave buoy that collects displacement data over time. The wave buoy closest to the site is PacIOOS Buoy 098 on the south side of Mōkapu headland, located at $21°24.85'$ N, $157°40.73'$ W and at a depth of 82 meters. The buoy collects the wave height, direction, and period in half an hour updates, which are available on the PacIOOS website[1].

Because the nonhXB model is depth-averaged, each computational grid has a corresponding depth value which is averaged from the area of that grid cell. The corresponding depth is found using bathymetry data. One bathymetry dataset for this project is obtained from the National Ocean and Atmospheric Administration (NOAA) Continuously Updated Digital Elevation Model (CUDEM). The NOAA Data Access Viewer provides the CUDEM data at a 1/9-arc second (3m) resolution and covers a significant amount of the east coast of Oahu. The vertical datum is the Mean Sea Level (MSL) and the coordinate system is the Universal Transverse Mercator (UTM). Another option for the bathymetry dataset would be to use 1-m resolution LiDAR data that was collected by the U.S. Army Corps of Engineers (USACE) (see Figure 2.1). The survey was conducted in 2013, spanning the island of Oahu. As the resolution is higher than the NOAA CUDEM, it could provide more accurate results. The bathymetry dataset is converted to a Network Common Data Form file (netCDF) using QGIS, an open-source geographic information system. The netCDF file can then be read into MATLAB for the numerical models, including the SWAN grid, nonhXB grid and many of the plots displaying results.

2.3 Numerical Models

2.3.1 XBeach Model Description

As previously mentioned, XBeach is an open-source software that is used for simulating nearshore hydrodynamic and morphodynamic processes provided by Deltares. It was selected for this project, as it is cost-effective and can produce results in a feasible timescale.

[1]https://www.pacioos.hawaii.edu/waves/buoy-mokapu/

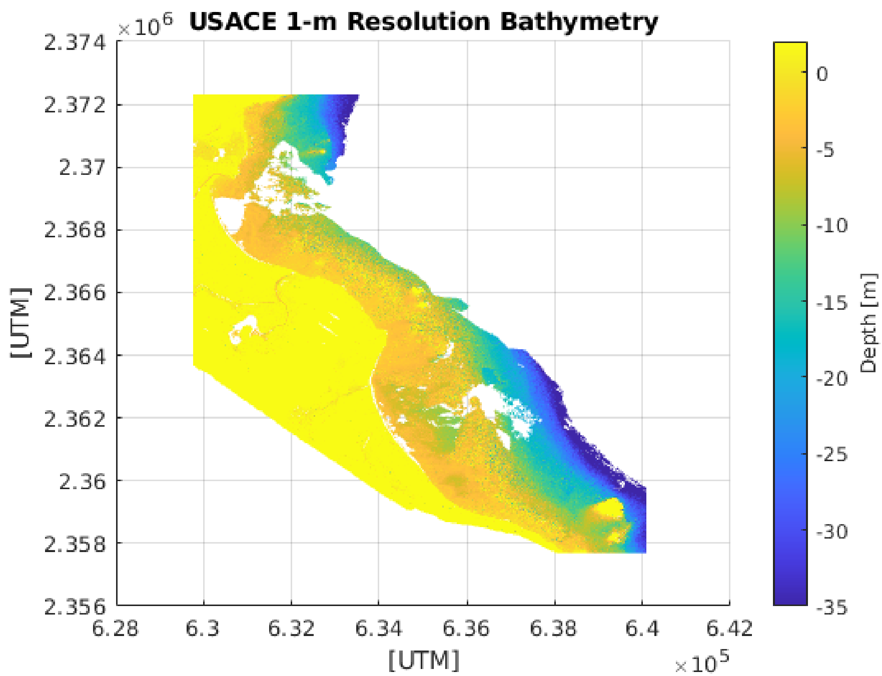

Figure 2.1 USACE 1-m Resolution Bathymetry Data

The model is depth-integrated and two-dimensional. The hydrodynamic aspect of the model includes short and long wave transformations, wave-induced setup and unsteady currents. The morphodynamic aspect of the model includes bed and suspended load transport, avalanching and bed updating. Much of the following information can be found in the XBeach User Manual, provided by Deltares.

There are three modes in XBeach: stationary, instationary (surfbeat) and non-hydrostatic. The stationary mode focuses on short-wave variations within wave groups, neglecting infragravity (IG) wave variations. The instationary or surfbeat mode addresses short-wave variations and includes IG variations. The non-hydrostatic mode employs a wave-resolving approach, solving the Nonlinear Shallow Water Equations (NLSWE) with a pressure correction term, allowing for the propagation and dissipation of individual waves. Because dispersion of waves is of significant importance for the project sites, the nonhydrostatic version will be used for this project.

Nonhydrostatic XBeach Description

The general model operates within the horizontal plane and has limitations in simulating wave overturning. NonhXB employs a momentum conservation scheme alongside depth-limited wave breaking criteria, which is further discussed in Section 2.5. The governing continuity and momentum equations for the basic one-layer, nonhydrostatic model are as follows (Smit et al. 2010; Stelling and Zijlema 2003a; Zijlema and Stelling 2008):

$$\frac{\partial \eta}{\partial t} + \frac{\partial (Hu)}{\partial x} + \frac{\partial (Hv)}{\partial y} = 0 \tag{2.1}$$

$$\frac{\partial u}{\partial t} + u\frac{\partial u}{\partial x} + v\frac{\partial u}{\partial y} + g\frac{\partial \eta}{\partial x} + \frac{1}{H}\int_h^\eta \frac{\partial p}{\partial x}\,dz = \frac{1}{\rho H}\left(\frac{\partial H\tau_{xx}}{\partial x} + \frac{\partial H\tau_{xy}}{\partial y} - \tau_{bx}\right) \tag{2.2}$$

$$\frac{\partial v}{\partial t} + u\frac{\partial v}{\partial x} + v\frac{\partial v}{\partial y} + g\frac{\partial \eta}{\partial y} + \frac{1}{H}\int_h^\eta \frac{\partial p}{\partial y}\,dz = \frac{1}{\rho H}\left(\frac{\partial H\tau_{yx}}{\partial x} + \frac{\partial H\tau_{yy}}{\partial y} - \tau_{by}\right) \tag{2.3}$$

$$\frac{\partial w}{\partial t} + u\frac{\partial w}{\partial x} + v\frac{\partial w}{\partial y} = -(p_\eta + p_b) + \frac{1}{\rho H}\left(\frac{\partial H\tau_{xz}}{\partial x} + \frac{\partial H\tau_{yz}}{\partial y}\right) \tag{2.4}$$

where (x,y,z) and t are the horizontal spatial and temporal coordinates respectively. η is the free surface elevation, H is the water depth and g is the gravitational acceleration. ρ is the density of water, which is kept as a constant salt water value, and q is the normalized dynamic pressure. The variables p_η and p_b are the dynamic pressure at the water surface and the bottom respectively, while (u, v, w) are depth-averaged flow velocity. The bottom shear stresses in the (x, y) plane are defined as τ_x and τ_y. These shear stresses are expressed in terms of ν_h, the horizontal viscosity. It is described by the Smagorinsky model, which uses eddy viscosity to represent the effects of turbulence at a scale smaller than the simulation grid resolution. It uses the strain rate of the resolved flow field to determine the amount of turbulent mixing and diffusion at a given domain location (Smagorinsky 1963). τ_x and τ_y are expressed as (Rijn 1993):

$$\tau_{bx} = c_f \rho u \sqrt{u^2 + v^2} \tag{2.5}$$

$$\tau_{by} = c_f \rho v \sqrt{u^2 + v^2} \tag{2.6}$$

where τ_{bx} is the shear stress in the x direction and τ_{by} is the shear stress in the y direction. ρ is the fluid density. The variables u and v are the velocity components in the x and y directions, respectively. Finally, c_f is a coefficient related to the friction factor and can be defined as:

$$c_f = \frac{gn^2}{H^{1/3}} \tag{2.7}$$

where n is the Manning coefficient.

A limitation of the nonhXB is that because it argues the NLSWE, its applications are limited in the shallow and intermediate depth range. The model domains extending beyond 30 meters of depth should be avoided, as it may cause instabilities within the simulation. The nonhXB also usually uses a single layer in the vertical direction, meaning there is a single cell of resolution in the water column. The reduced two-layer model divides the vertical layer into two to improve dispersion. The single layer formulation is valid up to a relative water depth (kh) of 1.2, while reduced 2-layer formulation is valid up to a relative water depth of 3 (Bai and Cheung 2016). A more in-depth study of the two simulation types and their suitability for the project site will be discussed in Chapter 4.

2.3.2 SWAN Model Description

As mentioned in the section above, XBeach simulations are not designed to handle deep water wave statistics and expanding the domain is computationally expensive. For this reason, XBeach is run in conjunction with the Simulating Waves Nearshore (SWAN) wave model. SWAN is a phase-averaged model, which is governed by the Wave Action Balance Equation with sources and sinks. SWAN can be implemented in a Cartesian or curvilinear grid coordinate system, which is helpful when covering large domains. As this project studies a relatively small area, the Cartesian system is chosen. The governing equation for Cartesian coordinates is (Mei 1983; Komen et al. 1994):

$$\frac{\partial N}{\partial t} + \frac{\partial c_x N}{\partial x} + \frac{\partial c_y N}{\partial y} + \frac{\partial c_\sigma N}{\partial \sigma} + \frac{\partial c_\theta N}{\partial \theta} = \frac{S_{tot}}{\sigma} \tag{2.8}$$

where N represents the wave action. x, y are Cartesian coordinates, t is time, θ is the propagation direction of the wave components. $c_x, c_y, c_\sigma, c_\theta$ are the propagation velocity in x-space, y-space, σ-space, θ-space respectively. $\frac{S_{tot}}{\sigma}$ represents the source term in terms of energy density. The first term on the left-hand side of Equation 2.8 is the rate of change of action density over time. The second and third terms are the propagation of action through physical space. Finally, the fourth and fifth terms represent how variations in depth and currents cause shifts in relative frequency and refraction. c_x, c_y can be defined as:

$$c_x = c_{g0} \cos\theta + U_x \tag{2.9}$$

$$c_y = c_{g0} \sin\theta + U_y \tag{2.10}$$

where c_{g0} is the group velocity dependent on depth and U is the currently velocity divided into x and y directional components.

The right-hand side of Equation 2.8 is the total source term, S_{tot}, and is given by:

$$S_{tot} = S_{in} + S_{nl3} + S_{nl4} + S_{ds,w} + S_{ds,b} + S_{ds,br} \tag{2.11}$$

Respectively, these terms represent wave growth by the wind, nonlinear transfer of wave energy through three-wave and four-wave interactions, wave decay due to whitecapping, bottom friction and depth-induced wave breaking.

The purpose of SWAN in this context is to handle the transformation between deep and coastal waters for nonhXB to use. As the buoy datum was selected to provide the information regarding the wave climate, the 82 meter contour from which the time series was taken is beyond the scope of XBeach. SWAN is implemented for the transition to nearshore statistics, meaning that if the study was conducted in shallow water or a wave flume SWAN would be redundant.

2.4 Numerical Model Setup

The XBeach model operates under the Cartesian coordinate within the Universal Transverse Mercator (UTM) system, which is divided into 60 zones of 6 degrees of longitude each. After selecting the area of interest, the domain is discretized into smaller cells to manage the computational load. These grid cells can vary in size and shape, either uniform (rectangular) or irregular. Characteristics such as dynamic pressure, bottom and free surface variables are defined at cell centers, while depth-averaged velocities are defined at cell interfaces. The collective region of the model domain, including grid cells, constitutes the numerical grid. XBeach requires a specific grid orientation, with the x-direction aligned to wave propagation and the y-direction aligned perpendicular to the wave propagation (McCall et al. 2015). Most commonly used as the boundary conditions for the model is a spectral input, derived by SWAN. SWAN takes a wave condition as an input and provides a wave spectrum that is implemented into nonhXB at the domain boundary.

2.4.1 Grid Setup

Both nonhXB and SWAN require an input file specifying the coordinates of each grid cell and a second file with the corresponding water depths in each cell. As aforementioned, there

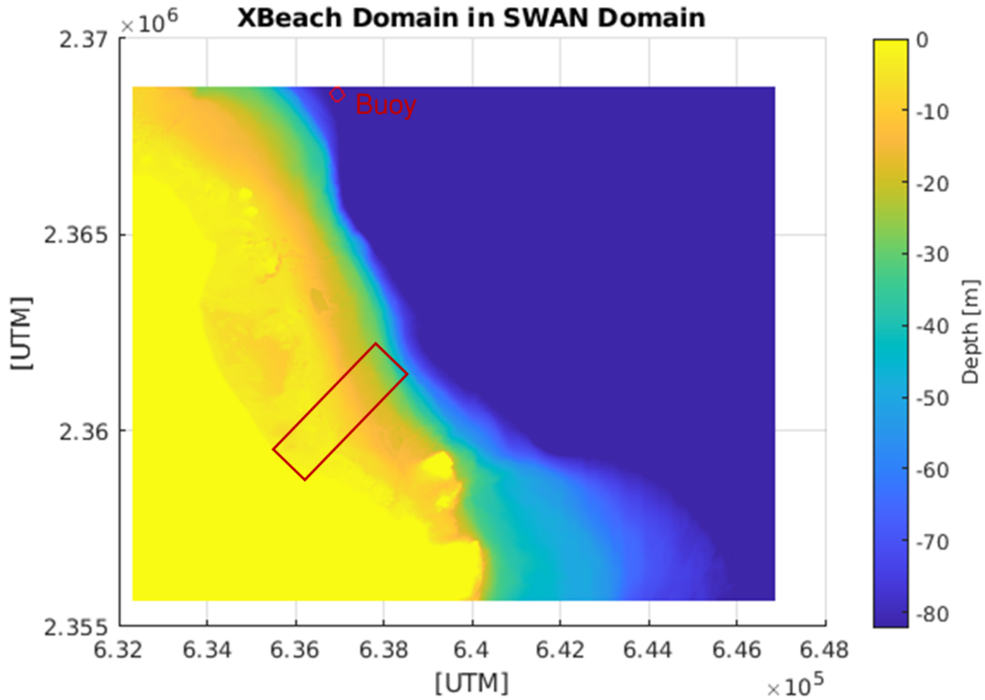

Figure 2.2 XBeach Domain (red) in SWAN Domain

are two important aspects of the SWAN and nonhXB domains: resolution and orientation. The resolution of the SWAN domain may be significantly lower (approximately 10 times) than that of the nonhXB domain because the primary focus of the study is nearshore. The nonhXB domain requires higher resolution to accurately simulate the wave conditions. Given that the precision of the results is not a critical consideration for SWAN, a uniform grid of 50 meters will be used. The other aspect, orientation, is crucial for the nonhXB domain but unimportant for the SWAN domain. As SWAN can force any side of the model boundary, the boundaries are set to allow wave action to move in and out of the domain. For the cases in this project, the north direction was set as the upper boundary. The nonhXB domain is required to be aligned so that the x direction is parallel to the mean direction of wave propagation. The angle at which the domain is oriented is found through an iterative process, which is discussed below. Figure 2.2 shows an example of the nonhXB domain within the SWAN domain.

XBeach Setup

The nonhXB grid is formed by defining the resolution of the grid cell in the x and y directions. The resolution is the most crucial and computationally expensive aspect of the numerical setup. If the resolution is too coarse, the simulation may fail to capture the wave characteristics. If the resolution is too fine, the simulation time will be unreasonable and instabilities may occur. Each grid cell of the grid is defined by the bathymetry and water depth at its coordinates. The 1-m resolution bathymetry from USACE was preferentially used for the nonhXB grids, however is missing data in certain areas of the eastern coast. The 3-m resolution bathymetry was implemented in cases where the coverage of the 1-m was insufficient. To ensure the bathymetry was smooth and caused no numerical instabilities, a smoothing filter was applied.

To define the resolution of the grid, a uniform scheme can be implemented, where the spacing between grid points is constant throughout the entire domain. The spacing should be sufficiently small to capture the wave characteristics, which can pose a challenge in terms of computational feasibility. As discussed in Chapter 1, the study done by Jacobs (2010) found that 30 grid points per wavelength is sufficient to capture the wave characteristic in a nearshore environment, whereas the thesis written by Chase (2023) found that 70 grid points per wavelength were preferable in terms of wave breaking results, despite increased computation time. The majority of the simulations run for this project were based on the 70 grid points per wavelength, as a precaution.

The other aspect that impacts the size of the nonhXB domain is the offshore boundary. To select the offshore boundary for the nonhXB grid, a depth should be such that the domain is not overly large, making the simulation computationally expensive, but large enough to allow the wave environment to be properly studied. Bai and Cheung (2016) suggest a location such that $kh \leq 3$ to avoid numerical instabilities, where kh is the wave depth parameter. All of the simulations run for this research implemented an offshore boundary depth contour of 30 meters. Though the domain size may impact the results, it is considered out of the scope of this project. The method to define the orientation, the other aspect of the nonhXB grid, is discussed in Section 2.4.2 and is driven by SWAN.

As discussed in Chapter 1, edge waves are of concern when studying IG waves. One primary mechanism for generating edge waves is resonance, which can occur when the wave environment is partially enclosed by headlands or is a bay. While Waimānalo Beach is located between two headlands, it is not feasible to simulate a domain size large enough to cover the entire bay. The second mechanism for generating edge waves is an oblique incident wave angle. The waves studied in this research have been found to be at an essentially incident angle at the coast. For these reasons, edge waves are not studied in this project.

SWAN Setup

As previously discussed, SWAN is used to generate the boundary conditions and define grid orientation for the nonhXB model. Set up in the same Cartesian coordinate system, the SWAN model takes a significant wave height, peak period and peak direction as input parameters of the wave climate. The SWAN grid is set up using the bathymetry datum from NOAA. As Buoy 098 is at around 82 meters of depth, the bathymetry beyond this point was smoothed to a constant depth to improve the performance of the wavemaker. The same smoothing filter applied to the nonhXB grid was used on the bathymetry in the SWAN grid.

SWAN most commonly uses a JONSWAP spectrum with a peak enhancement factor, which controls the variability in wave frequency for the spectrum (Hasselmann et al. 1973). For this project, a user-defined spectral input from pacIOOS buoy 098 was implemented to better represent the wave climate (see Section 4.1. The boundaries for SWAN are set up such that the waves can propagate in and out of the domain, with north and east being the most common directions for this project. Once the parameters are set, the SWAN grid at a 50 meter resolution is run to output the file that includes the significant wave height, peak period and peak direction for the nonhXB boundary conditions.

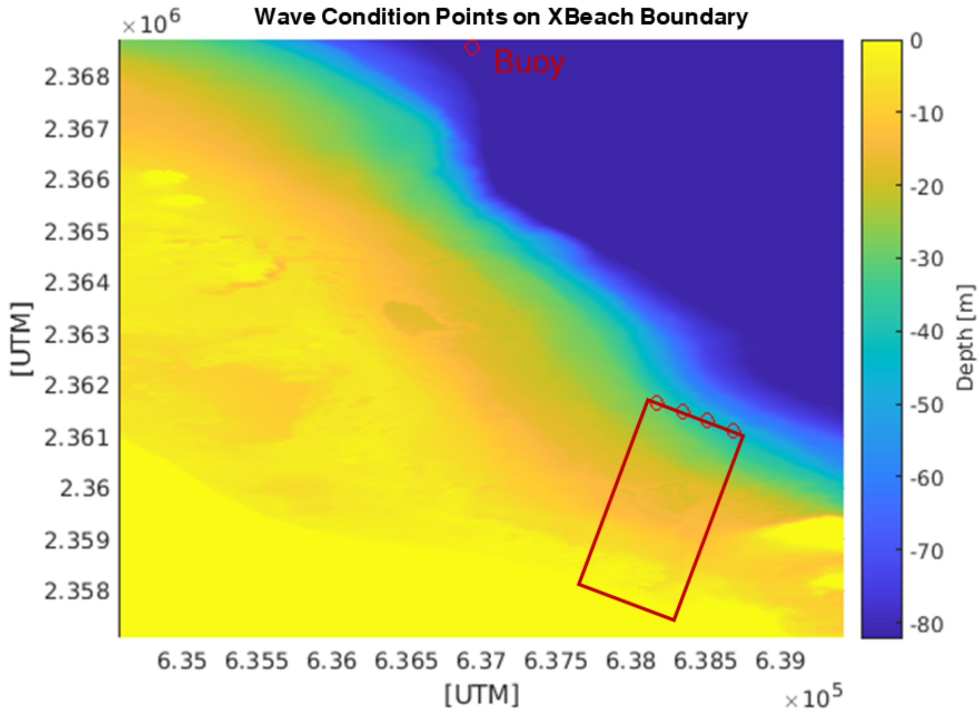

Figure 2.3 Example of Boundary Input (where red circles are SWAN spectral input points)

2.4.2 One-way Model Coupling

Once the SWAN run is complete, the results can be implemented into the nonhXB grid. A series of points are selected along the depth contour of the offshore boundary to define the simulation's boundary conditions. The coordinates of these points are saved in a separate file to the grid and added as an input for a secondary SWAN run that provides additional information at the boundary. An example of these points along the nonhXB boundary can be seen in Figure 2.3. As discussed, the orientation of the nonhXB grid is crucial and must be aligned with the wave direction at the boundary. If the two are not aligned, the simulation may terminate due to alongshore propagation. The results of the SWAN simulation are what drives the orientation of the nonhXB domain, therefore the output of SWAN (the mean wave propagation) is compared to the initial angle of nonhXB grid. The peak directions at the points specified in the secondary SWAN run are averaged to one value and are then compared to the orientation angle of the nonhXB grid. Refraction in the

SWAN model makes it so the input wave direction is different from the average direction found at the boundary. The nonhXB domain must be reoriented and SWAN rerun until the two line up at a 1 degree threshold.

Once the nonhXB grid is correctly oriented, the SWAN simulation can provide a wave spectrum at the nesting points in the form of a .sp2 file. Spatially-varying spectral boundary conditions in nonhXB require multiple spectral definition files with corresponding location files, therefore the .sp2 file is parsed into each nesting grid location. An additional file is required to inform the simulation which location file is intended for each spectrum file (SWAN-Team 2006).

2.4.3 Simulation Implementation

Once the nonhXB grid and its boundary conditions are properly defined, a run file must be prepared to inform the simulation of what parameters to set up. The file, called params.txt, is a list of keywords that define the conditions for the simulation. Physically processes, such as sediment transport and wave current interactions, can be defined in this file, as well as settings such as the type of model or which output variables. The spectral file described in the Model Coupling Section and the grid files are specified in the params.txt. The Courant-Friedrichs-Lewy (CFL) number is also set in the input file. The CFL number determines the time step for the simulation, where a lower number decreases the time step and generally increases simulation time. The default maximum CFL number for nonhXB is 0.7, however many of the simulations in this project were run at a lower number (0.3-0.6) to ensure numerical stability (McCall et al. 2022). All simulations were set with a hydrodynamic start time of 0 seconds and a still water level of 0 meters, unless stated otherwise. Beach morphology and sediment transport were not studied in this project.

Each simulation was run for at least 500 wave cycles, to minimize the effects of random seeding at the offshore boundary. An additional 15 percent of the total time was included to allow for the simulation to stabilize. The maximum time simulated in this research is 3 hours (10800 seconds), with the majority of simulations being run for 1 hour (3600 seconds).

This is due not only to the time it would take to achieve results but also due to the size of the output file. Two computers were used for the duration of this project, with a maximum Random Access Memory (RAM) of 126G. Simulations exceeding 1 hour, or 3 hours with a small domain, were unable to be processed due to the RAM limitation. Each simulation outputs the time series for the surface elevation and breaker index. The variables were all output in NetCDF formatting.

2.5 Probability of Wave Breaking

Wave breaking is an inherently complicated and dynamic process, making it difficult to model. As a wave approaches the shore, the nonlinear interactions with other waves impact where the wave may break. Factors such as bottom roughness, current interactions and wind also impact the nature of a breaking wave. For these reasons, representing the breaker climate is most effectively done using the probability of waves breaking, rather than finding the locations of breaking waves in an area of interest.

In XBeach, wave breaking is found by applying a hydrostatic front approximation, which enhances the accuracy in predicting the location and intensity of wave breaking and dissipation. The model treats breaking waves as hydrostatic bores by removing nonhydrostatic terms when waves reach a predefined breaking threshold. In the nonhXB model, the pressure distribution beneath the bore is considered hydrostatic when surface breaking exceeds a certain value. This hydrostatic bore reverts to a wave once a specified reform steepness parameter is reached, allowing it to propagate and break again according to a secondary wave steepness parameter. The steepness parameters are part of the nonhydrostatic correction and are considered advanced options. For this reason, McCall et al. (2022) suggest the default values are used (max steepness of 0.6 and reform steepness of 0.25+maxbrsteep). As discussed in Section 2.4.3, the breaker index is an output variable for each simulation. This parameter, denoted as *gamma*, quantifies the ratio of wave height to water depth at which waves break. The nonhXB model determines wave breaking by assigning each grid cell a value of 0 (no breaking) or 1 (breaking occurs).

The probability of breaking can be defined as Equation 2.12:

$$Q_b = \frac{N_{breakers}}{N_{waves}} \tag{2.12}$$

where Q_b is defined as the probability of breaking and N is the number of waves. To find the number of breaking waves in a simulation, a logic statement is used to find the grid points where the index changes from 0 to 1. The count is made at the transition between 0 and 1 to ensure each wave is counted only once.

To find the total number of waves in the simulation, a zero-upcrossing analysis is used, an example of which is in Figure 2.4. The zero-upcrossing method uses the mean water level (MWL) as a baseline. If η, the water surface elevation, crosses below the line it is treated as a negative value and above the line is treated as a positive value. The time step at which η crosses the MWL from negative to positive is recorded. The time at the following instance in which η repeats this crossing is also recorded. The difference between the two is a single wave period. A similar process is used to find the single wave height, in which the maximum and minimum values of η are recorded and the difference is found. By continuing this method for the length of the time series, the complete wave state can be found.

Once the total number of individual waves are detected in the zero crossing method, the fraction of waves that are breaking can be calculated using Equation 2.12 for each grid point of the simulation results. The grid point indices associated with each probability can then be mapped across the project site and used as a measurement of the wave transformations.

2.6 Spectral Analysis

Wave spectra are used to describe the distribution of wave energy across different frequencies, or power spectral densities (PSDs). From a spectrum, several wave parameters can be derived, such as significant wave height, peak wave period, and mean wave direction,

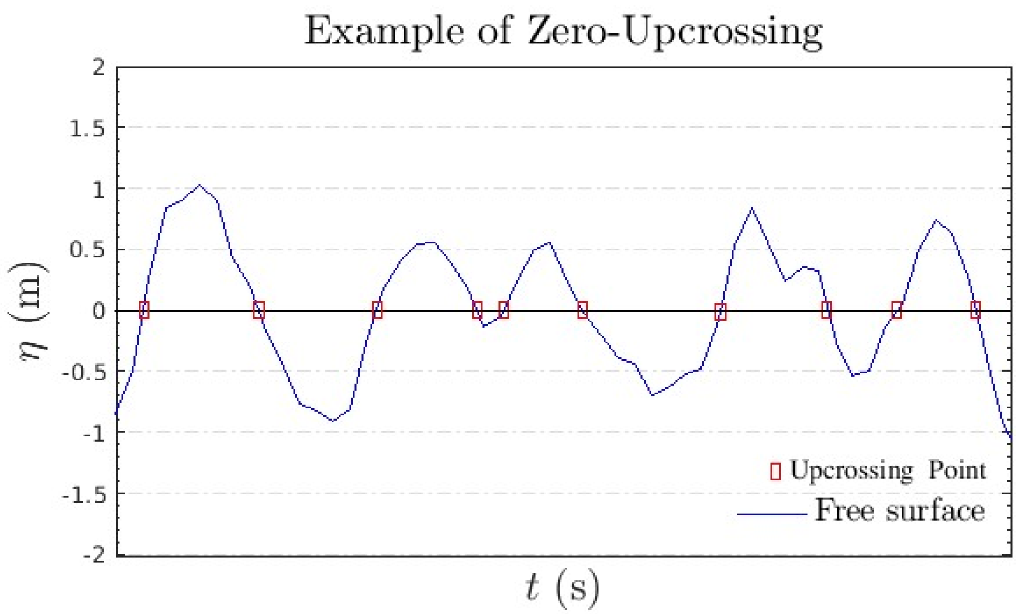

Figure 2.4 Example of Upcrossing Method

so that the wave climate can be better understood. One type of PSD, Welch's Method, estimates the power spectra by dividing the time signal into smaller segments with a certain percentage of overlap. For this project, 50% overlap was implemented. Each time segment is windowed to minimize spectral leakage then a Fast Fourier Transform (FFT) is applied to calculate the periodogram. The periodograms are then averaged to produce a smoother spectrum of the wave climate (Rossi et al. 2020). From the wave spectrum, the power of random waves can be calculated.

$$P = \rho g \int_0^\infty S(\omega) C_g(\omega)\, d\omega \tag{2.13}$$

where ρ is the density of seawater, g is gravitational acceleration, $S(\omega)$ is the wave energy spectrum, and $C_g(\omega)$ is the group velocity. Calculating the wave power at given points in a simulation domain allows for a better understanding of the wave evolution in the nearshore environment.

2.7 Field Observations

To compare the results of the nonhXB simulations, a field observation was conducted. The study took place at Waimānalo Beach, Oahu, Hawai'i on October 20, 2023. The focus of the study was measuring the water surface elevation, as it is a key nonhXB output variable. Surface elevation can also be measured using pressure sensors in the field. By comparing the modeled water surface elevations with the actual pressure sensor data, the study aimed to validate the accuracy of the simulated wave characteristics. To measure the water surface elevation in the field, HoboWARE pressure transducers were deployed at several points in the Waimānalo Beach area for a 4 hour duration[2]. The sensors recorded a time series of absolute pressure, allowing for a detailed comparison between the observed and simulated data. The details of the study are discussed in 3.

One significant limitation posed by the boundary conditions of the nonhXB model is that it is unable to simulate more than one wave condition simultaneously. Because of this, the wave conditions selected for the field observations need to be ideally limited to one swell for comparison or averaged over time to have one input.

2.7.1 Data Processing

The data were offloaded from the pressure transducers using the HOBOware software, where it can then be exported as a .csv file. As the raw datum is the absolute pressure over the collection period, it must be processed to be compared correctly with the simulation values. The absolute pressure is the sum of the hydrostatic and dynamic pressure, therefore the mean value must be removed. The mean represents the static pressure due to the water column's weight, or the hydrostatic pressure. By removing the hydrostatic pressure, the variation in pressure caused by movement in the water can be studied (dynamic pressure). The data must be converted to their equivalent sea surface elevation. The hydrostatic

[2] https://www.onsetcomp.com/products/data-loggers/u20-001-04?v=U20-001-04gad$_{source} = 1gclid = EAIaIQobChMIlYXmoe6ihwMVDBWtBh1GSA2yEAQYAiABEgJuVfD_BwE$

equation for pressure was used.

$$P = \rho g \eta \tag{2.14}$$

where ρ is seawater density, g is gravitational acceleration and η is the free surface elevation. After solving for η, the time series for water elevation over the data collection time was found.

2.7.2 Wave Buoy 098

As aforementioned, a wave buoy is located near the project site and can be used to help characterize the wave climate. Pacific Islands Ocean Observing System (PacIOOS) provides wave observation data throughout the Pacific Ocean using a series of wave buoys. Each buoy collects the wave height, direction, and period in half an hour updates. The buoy datum is additionally distributed through the Coastal Data Information Program (CDIP), which provided the dataset collected by a buoy for this project. The buoy most relevant to this project is PacIOOS Buoy 098. The CDIP dataset was provided for the day of the pressure sensor deployment, October 20, 2023, at a sampling frequency of 1.28 Hz. Sample time in UTC, as well as the meters of displacement in the N/S, W/E and vertical directions make up the data. The file format is netCDF and was accessed using MATLAB. A section of the raw data can be found in Appendix B. The sample time was converted into seconds and processed in the same method as the pressure sensors.

Chapter 3

Field Observations of Waimānalo Beach

3.1 Field Survey

A preliminary study was carried out at Waimānalo Beach on October 20, 2023. The purpose of the observations was to have a method of comparing the nonhXB simulation results to measured data at the same site, as discussed in Chapter 2. The bathymetry of the project site is shown in Figure 3.1. The following section outlines a description of the study, with further details available in Appendix A.

Three locations were selected along the beach and a team of 5 members, including 2 free divers, were deployed to collect field data. Five total HOBOware pressure sensors were calibrated and programmed to collect data for a 6 hour duration at a frequency of 1 Hz. One pressure sensor was placed on shore to measure barometric pressure (Location 1), as a method of compensating for the effects of atmospheric pressure on the water column. Additionally, two pressure sensors were deployed at the same location (Location 4) as a control measure. The locations of the sensor drop sites can be seen in Figure 3.1, as red markers. The sensors remained in the water for a total of 4 hours each before being recovered by the free divers. Table 3.1 is a summary of the field deployment.

As seen in Table 3.1, the two sensors placed at Location 4 were not able to be recovered. The location is marked with an X in Figure 3.1. These sensors were placed in relatively shallow, high-energy water and were not attached to a surface buoy. Both sensors were

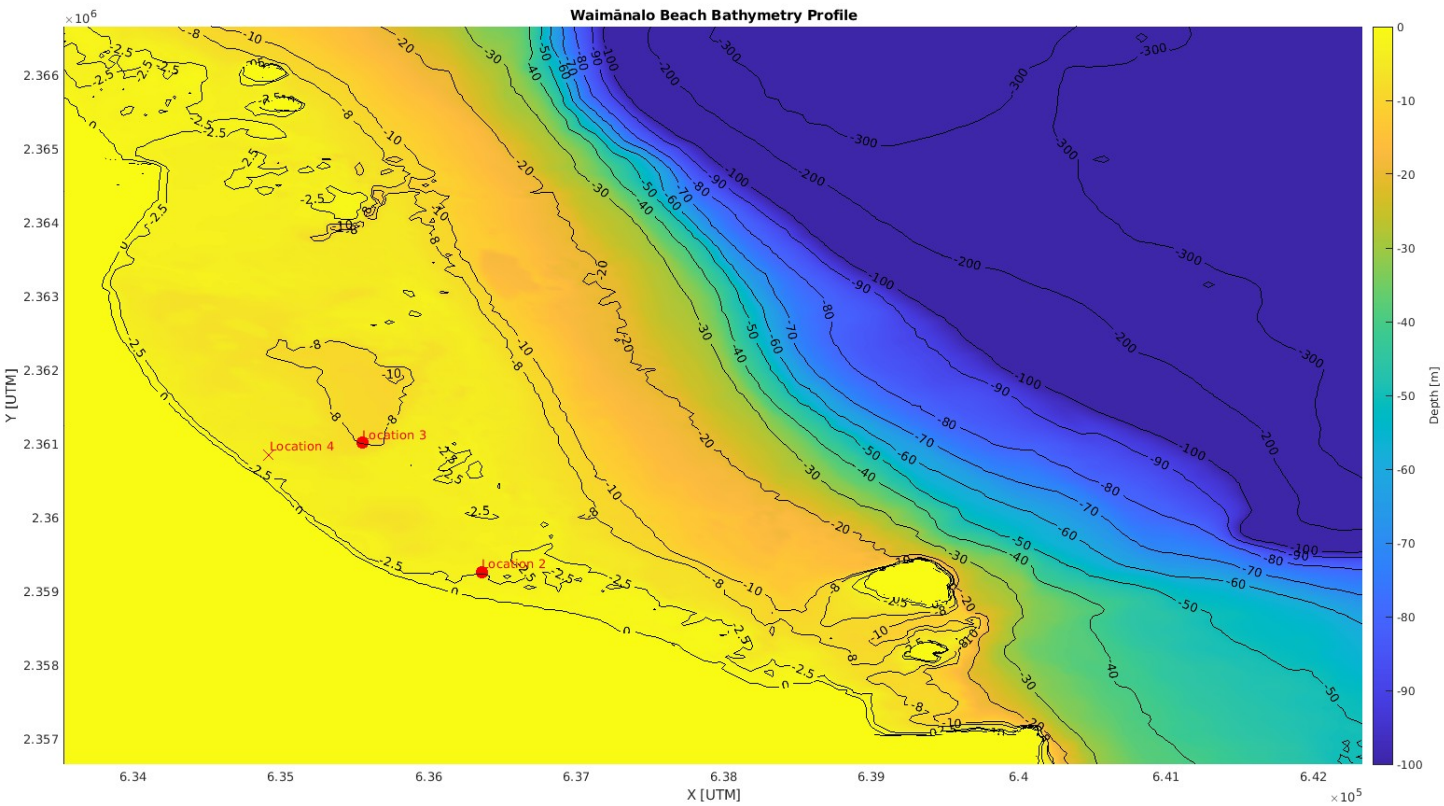

Figure 3.1 Waimānalo Beach Bathymetry Profile

Location	Notes	Latitude	Longitude	No. of Sensors	Depth [m]
1	Barometric pressure	N/A	N/A	1	-
2	Waimānalo Beach Park	21.330268	-157.685167	1	2.5
3	North Waimānalo, Intermediate Water	21.344525	-157.694822	1	8.0
4	North Waimānalo, Shallow Water	21.344758	-157.698867	2, both missing	2.0

Table 3.1 Summary of Pressure Sensor Deployment at Waimānalo Beach

displaced sufficiently far enough from the buoy that recovery efforts by the free divers were not possible. The sensors that were able to be recovered produced results that will be discussed in Section 3.3.

3.2 PacIOOS Wave Buoy 098

As discussed in Chapter 2, an additional method of characterizing the wave climate at the project site would be to use a wave buoy. PacIOOS 098 is the buoy most relevant to this project and its location in relation to Oahu can be seen in Figure 3.2, at a depth of 82 meters. It has coordinates of $21°24.85'$ N, $157°40.73'$ W, approximately 8 kilometers NNE from the location of the pressure transducers.

In this section, the wave buoy can provide a supplementary data source for the day the field survey took place. CDIP, one of the data distributors, provided the displacement time series at a sampling frequency of 1.28 Hz for October 20, 2023 [1]. The time series is in a netCDF file format and was read into MATLAB to display the time series and calculate the wave spectrum. The data were converted into seconds and cropped to a similar time window as that of the pressure sensors to derive the time series, which can be seen in Figure 3.3. The gap in the data is due to a 30 minute period where the data transfer between the buoy and data collection system was unsuccessful. To find the wave spectrum at the buoy Welch's Method was applied. As discussed in Section 2.6, Welch's Method is an approach used to quantify the wave energy distribution over a given area. The spectral results are shown in Figure 3.4.

[1] Dataset provided by Corey Olfe at UCSD

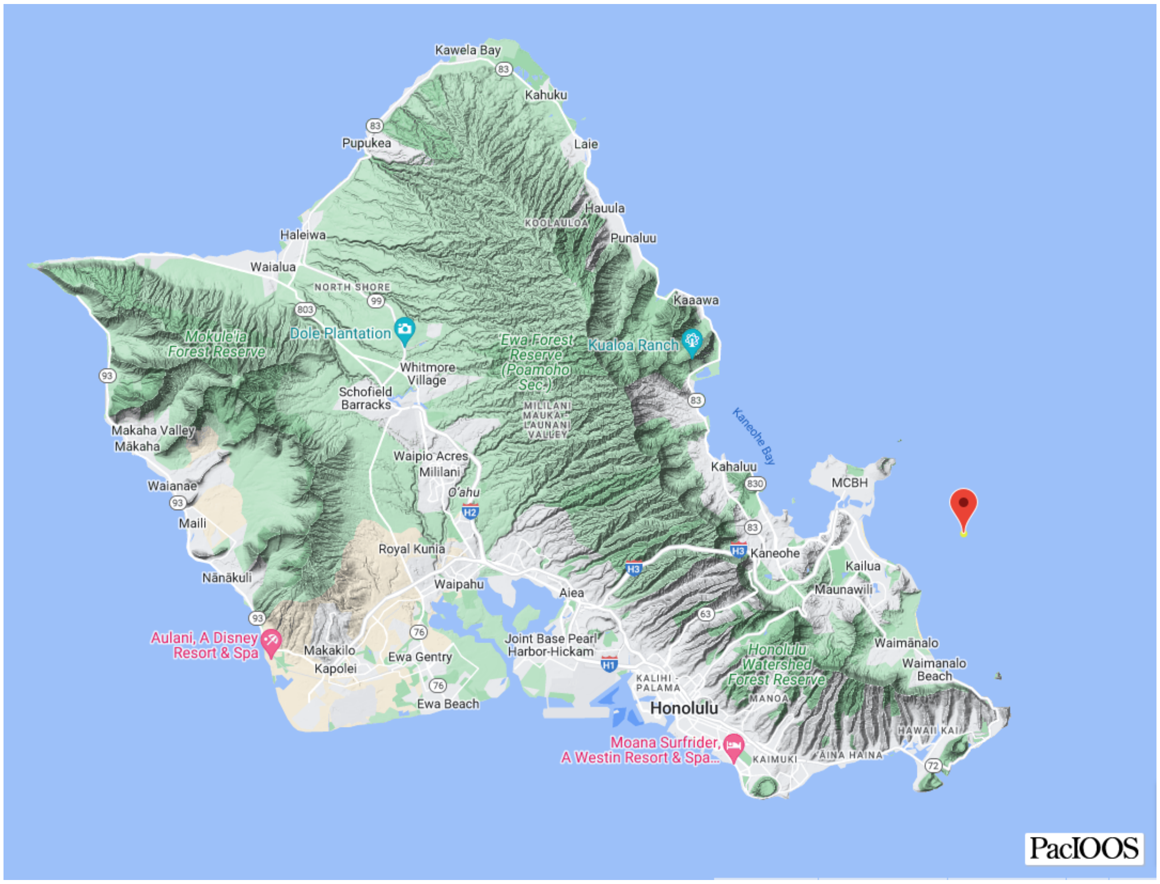

Figure 3.2 Location of PacIOOS Buoy 098

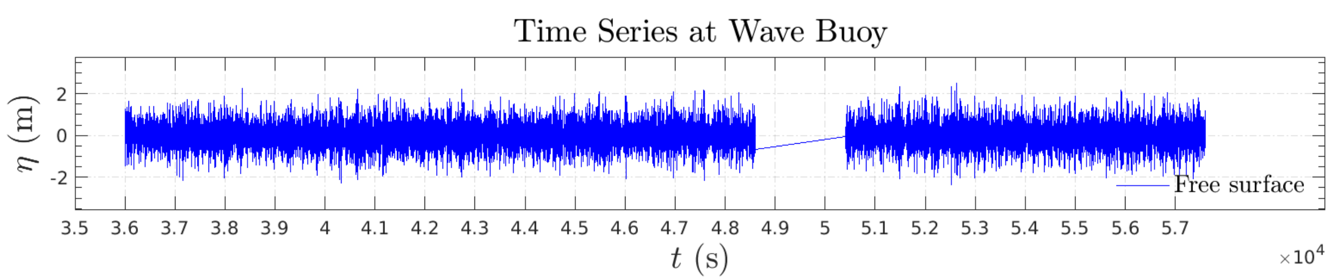

Figure 3.3 Time Series of Wave Buoy 098

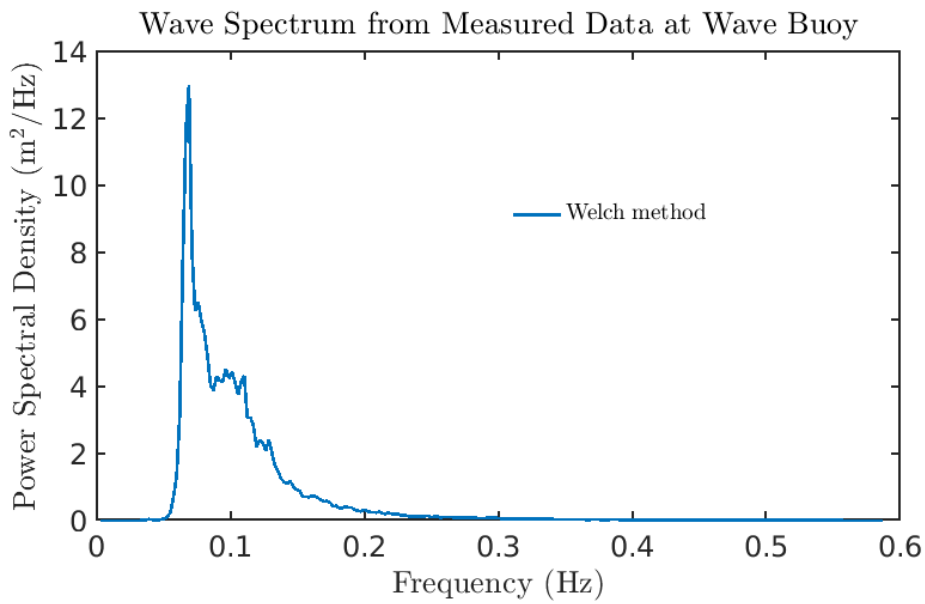

Figure 3.4 Wave Spectrum of Wave Buoy 098

3.3 Waimānalo Beach Survey Results

3.3.1 Time Series

Since the pressure sensors at Locations 2 and 3 were successfully retrieved, the data were offloaded using the HOBOware software. The raw data include absolute pressure and temperature over time. An example of this file can be found in Appendix B. The data were then processed to study the wave climate, using the method described in Section 2.7.1. Once the dynamic pressure was isolated to provide the time series, the data were cropped to a time window that reflected the duration of when the pressure transducers were in the water undisturbed, rather than the 6 hours they were programmed to collect for, which included deployment and recovery. Figures 3.5 and 3.6 display the final time series results for Location 2 and 3, respectively.

3.3.2 Spectral Analysis

The Welch's Method was applied to the data collected at Locations 2 and 3, which can be seen in Figures 3.7 and 3.8, respectively.

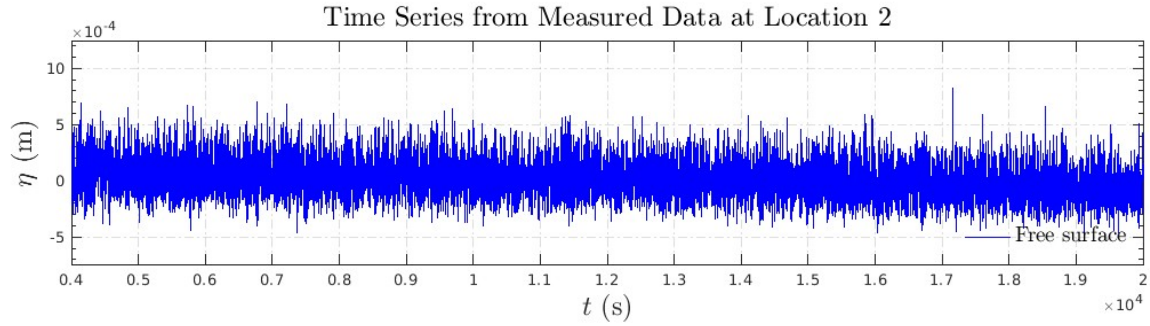

Figure 3.5 Time Series of Location 2

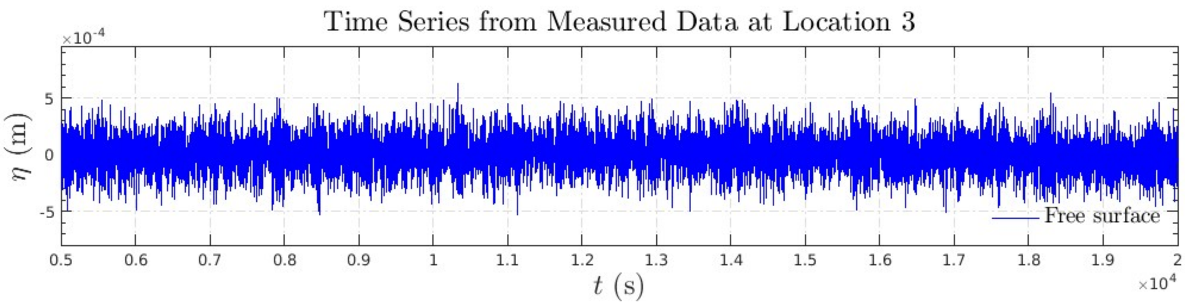

Figure 3.6 Time Series of Location 3

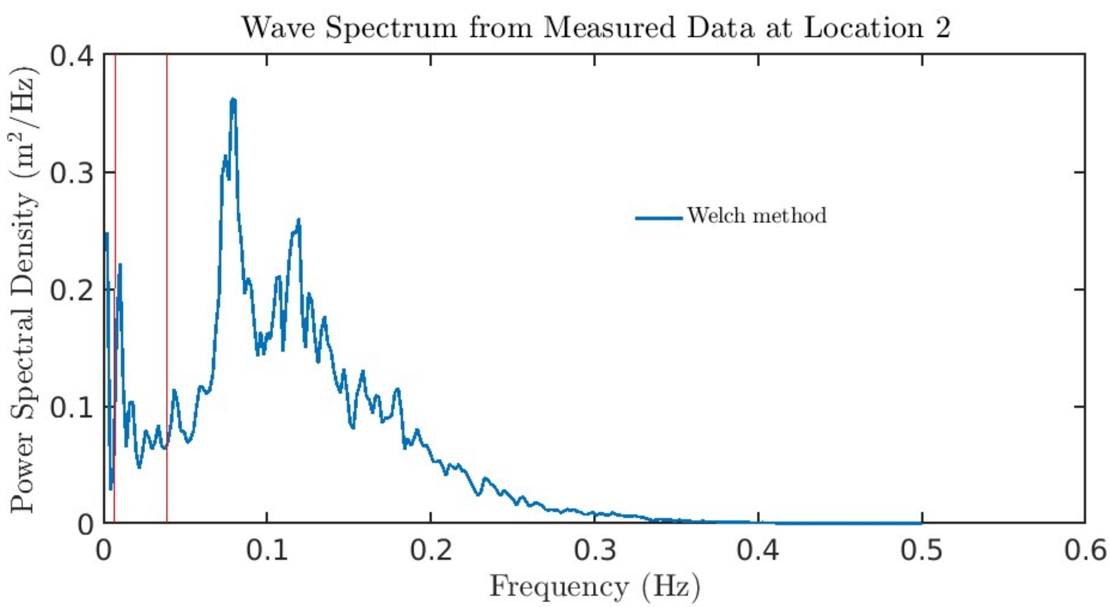

Figure 3.7 Measured Wave Spectrum of Location 2 (red lines indicate window of IG wave frequencies, where the period of the peak indicates IG is 102 seconds)

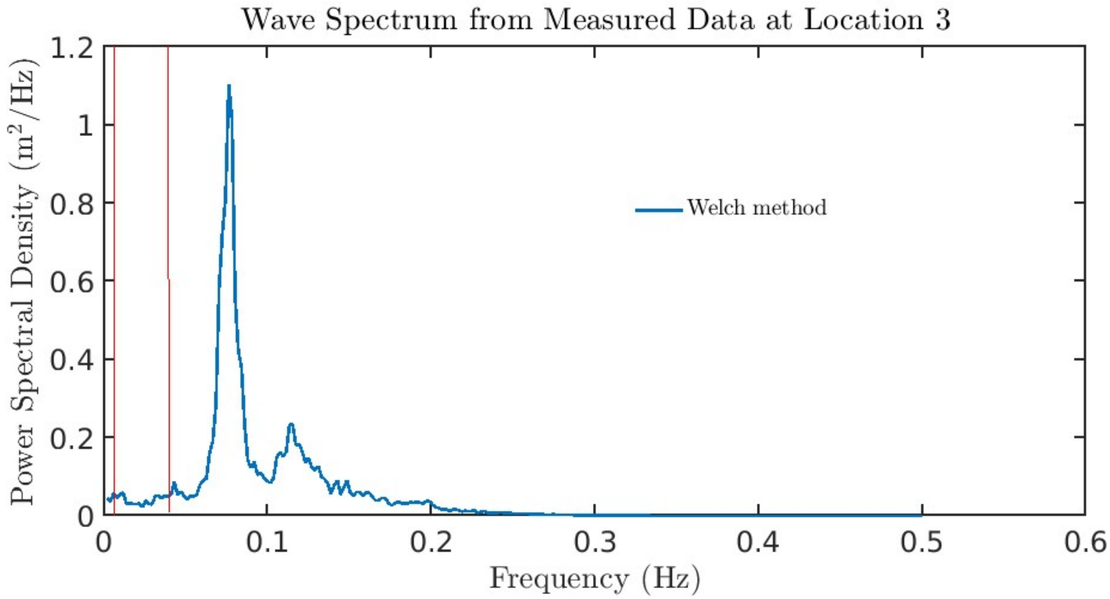

Figure 3.8 Measured Wave Spectrum of Location 3 (red lines indicate window of IG wave frequencies, where the period of the peak indicates IG is 85.40 seconds)

	Peak Period (s)	Secondary Period (s)	IG Wave Period (s)
Location 2	12.80	8.53	102.40
Location 3	12.80	8.83	85.40
Wave Buoy	14.55	13.22	-

Table 3.2 Periods Observed in Wave Spectra

3.3.3 Measured Data Results

The peak period, secondary period and IG wave period captured in the wave spectra for all three locations of measured data can be seen in Table 3.2.

The peak period measured at Location 2 and Location 3 is the same, 12.80 seconds. The secondary periods are also similar, with an average of 8.68 seconds. At the wave buoy, the largest peak period is measured at 14.55 s, with a secondary peak of 13.22 s. The red lines in the wave spectra plots represent the minimum and maximum frequencies of IG waves (0.004-0.04 Hz). The line is not included in the wave buoy figure, as no IG waves are evident. IG waves apparent at Location 2, with a peak period of 102.40 seconds (Table 3.3.3). At Location 3, the presence of IG waves is not as obvious as at Location 2, however there is a peak in the spectral density at a period of 85.40 seconds.

Location	Power (m^2/Hz)
Location 2	1.251e+03
Location 3	1.910e+03
Wave Buoy	3.722e+04

Table 3.3 Wave Power at Locations of Interest

The differences in period between the pressure transducers and the wave buoy may be caused by physical mechanisms that were not studied during the field observations. The pressure transducers did not capture the current or the nonlinear wave interactions that occurred during the collection window, which may contribute to a transfer of wave energy between different frequencies. Furthermore, it is unlikely to be attributed to the difference in sampling frequency. The sampling frequency of the pressure sensors is 1 Hz per cycle, or 1 second per cycle. The sampling frequency of the wave buoy is 1.28 Hz per cycle, or 0.7813 seconds per cycle. This conclusion is based on the Nyquist theorem, which states that if the sampling frequency is double that of the highest critical frequency components, it can be accurately captured (Vaidyanathan 2001). The criteria are met at Locations 2, 3 and the wave buoy.

The power was then calculated using Equation 2.13 based on the spectra that were found at each location. It was found that as the depth decreased, the power also decreased. As waves break and the energy is dissipated due to physical characteristics, such as bottom roughness, the power should decrease when moving towards the shore.

Chapter 4

XBeach Simulations

The following chapter outlines several parameters that have a significant influence on the results of the nonhXB model. First, the single layer and reduced two layer formulations are applied to the project site to determine which model is most suitable. Then, the effects of bottom roughness are explored. Three different Mannings coefficients are implemented while the numerical grid is kept constant to better understand how the bottom friction influences the wave transformation. Using the selected model formulation with the calibrated bottom roughness, the nonhXB results are compared with the results of the field survey. Additional Mannings coefficient values will be tested to explore the influence of bottom roughness on the presence of IG waves.

4.1 User-defined Spectral Input

As discussed in Chapter 2, SWAN is used to generate the offshore boundary for the nonhXB numerical setup. It most commonly takes a significant wave height, peak period and direction as input for the wave climate, then implements a JONSWAP spectrum to simulate the wave transformations. While JONSWAP is able to represent wind-generated waves well, it is a single peak spectrum. As seen in the results of the field observations (Figures 3.7 and 3.8), the spectra have multiple peaks. For a more accurate representation of the offshore wave climate, the spectrum for the time series collected from PacIOOS Buoy

098 on the day of the field observations was calculated. It was then implemented as the SWAN boundary. As SWAN makes the transformation from deep water to the 30m depth contour, a more accurate spectral representation may improve the accuracy of the nonhXB simulation results. All of the simulations in this section are conducted with this user-defined spectral input. The average peak period of the time series at Buoy 098 is 14.55 seconds, with a significant wave height of 2.41 meters. These parameters were calculated from the time series collected at Buoy 098, resulting in a relative water depth, kh, of 6.20.

4.2 Bottom Roughness Parameter

As discussed in Section 1.3, bottom roughness has a significant impact on the way waves evolve towards the shore. Using the equation for Mannings to represent bottom roughness is the default setting in nonhXB, however literature shows the suggested value of 0.035 for fringing reef environments may not be sufficient in a modeling context. As the Mannings equation is empirically based on uniform, open-channel flow, the value may need to be increased to accurately reflect the non-uniform flow experienced in the nearshore reef environment. Additionally, the wave boundary layer, which is responsible for wave energy dissipation, is not considered due to depth integration. Artificially increasing the Mannings value to an unrealistic value to better represent the bottom friction and dissipation causes the value to act more as a fitting parameter with no physical meaning.

To investigate what fitting value may best represent the project site, a baseline Mannings value was selected using on a study conducted on the east side of Oahu. The research implemented bottom friction values from a field survey to a wave model called STWAVE, which is phase-averaged. The study deployed Acoustic Doppler Velocimeters (ADVs) along the length of the site to collect wave data over 22 days (August-September of 2005). A range of Mannings values was then tested to determine which coefficient best aligned with the field survey results. A value of 0.2 was found to be most suitable as a baseline (Cialone and Smith 2007).

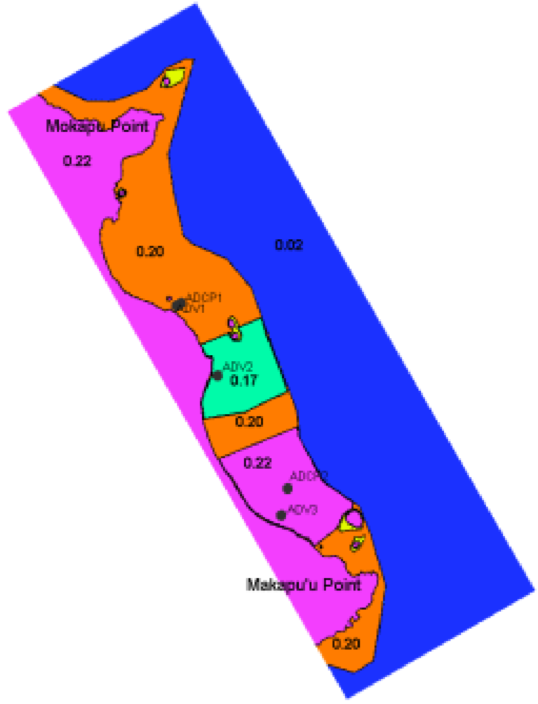

Figure 4.1 Map of Mannings Coefficients for the East Side of Oahu (Cialone and Smith 2007)

An additional component of the field survey was to collect data on the reef coverage of the study area. Using these results, as well as the initial simulation performance, Manning's values were applied in sections along the coast. The zones can be seen in Figure 4.1, where the primary point of interest for this project is assigned a Mannings coefficient of 0.22. Additional simulations were run using the coefficients based on the observed state of the reef. They were then compared to the ADV results, in addition to the readings from PacIOOS buoy 098. The simulations were found to be between 95-97% agreement (Cialone and Smith 2007). STWAVE is a phase-averaged model, whereas nonhXB is phase-resolved. Though this may impact the implementation of the Mannings value if it had physical meaning, it acts more as a fitting parameter in this project.

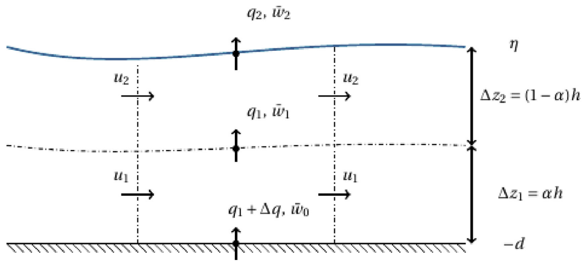

Figure 4.2 Vertical Layer Definitions for nonhXB (de Ridder et al. 2021).

4.3 One-Layer and Reduced Two-Layer nonhXB Formulation

The basic equations that make up the one-layer model were described in Chapter 2. The following section will provide the differences in the two-layer model and outline the simulations conducted to study in the difference in results.

4.3.1 Layer Model Formulation

The difference between the one and reduced two-layer models is the number of vertical layers in the water column. While the one layer model keeps the water column as a single unit, the reduced two-layer argues the dynamic pressure profile using two linear segments with a predefined pressure ratio (see Figure 4.2). Additional layers cause significantly higher computational expense as a result of the increased matrix system, as the matrix grid points multiply by each layer employed (Jacobs 2010). Deltares developed the reduced two-layer model of nonhXB to retain some of the dispersive behavior of the regular two-layer while maintaining a feasible computation time. It is reduced such that the nonhydrostatic pressure remains constant in the lower layer and the vertical velocity between the layers is neglected (McCall et al. 2022). The balance between improved simulation results and computational expenses is important to feasibility, therefore the two models are tested at the Waimānalo Beach site. The single layer formulation is valid up to a relative water depth (kh) of 1.2, while reduced 2-layer formulation is valid up to a relative water depth of 3 (Bai and Cheung 2016). Both of these values are much smaller than the kh of 6.2 at the water buoy, hence

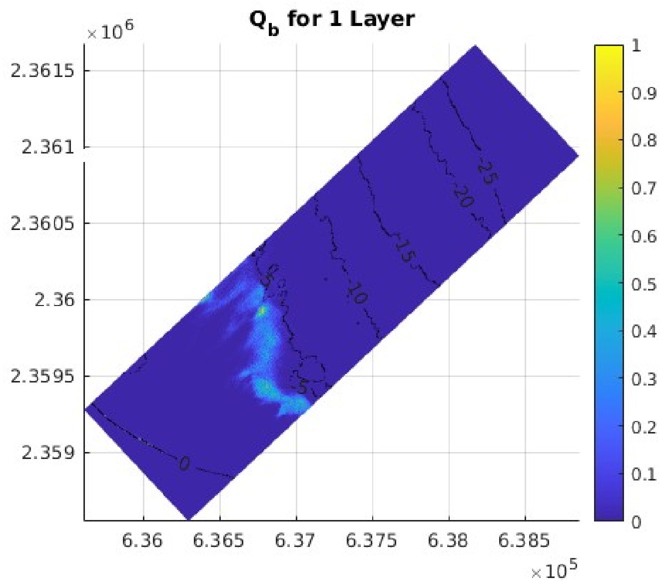

Figure 4.3 Probability of Breaking for 1 Layer Formulation (Mannings n = 0.22)

the need for SWAN. The offshore boundary conditions nonhXB are not produced along a given depth contour, rather at the angle of the incident wave. As the depths vary along the boundary, so does the relative water depth. The range found based on the SWAN results for both Locations 2 and 3 was 0.86-1.11.

4.3.2 Simulation Comparison

To study the impact of using a one-layer model in comparison to a two-layer model, a simulation using each model type was run. A 1.5 meter uniform grid was implemented and all input parameters were kept constant, apart from the number of layers used. As a Manning's coefficient value of 0.22 was suggested for the project site, it was used for both simulations. The probability of breaking for both formulations can be seen in Figures 4.3 and 4.4.

The probability of breaking maps show that the reduced two-layer formulation produces a higher Q_b in comparison to the single layer formulation. This may be due to the improved dispersion in the reduced two-layer model, as it can better capture the changes in wave energy distribution as waves move from deeper to shallower regions. Maintaining more

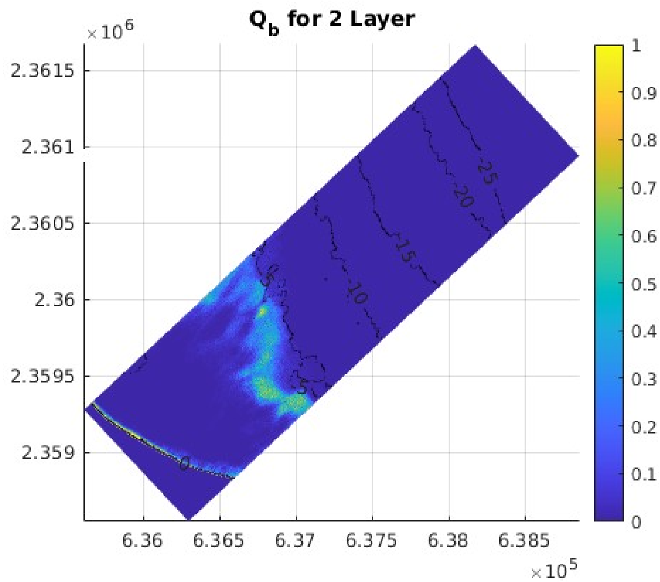

Figure 4.4 Probability of Breaking for 2 Layer Formulation (Mannings n = 0.22)

energy into the breaker zone would result in a higher probability of waves breaking within that region. The basic dispersion for the single layer formulation may cause Q_b to be underestimated. The increased Q_b translates to a decrease in wave energy shoreward of the breaker zone, which is reflected in the wave spectra calculated at Location 2 for the two model formulations (Figures 4.5 and 4.6). While the peak period remains the same for both types of model, the magnitude of the power spectral density is different. The reduced two-layer model results in a lower magnitude (0.455 m^2/Hz) at the peak than the single layer (0.486 m^2/Hz). Both the single layer and reduced two-layer models overestimate the magnitude of the power spectral density at the peak period in comparison to the measured spectrum (0.363 m^2/Hz). This may be due to the grid resolution implemented in the numerical scheme. According to Chase, selecting a grid resolution that is too coarse for the wave environment may cause the probability of breaking to be underestimated (Chase 2023). Increasing the grid resolution is known to be computationally expensive, which is also a concern of using the reduced two-layer formulation. Table 4.1 summarizes the differences in the computational expense between the two models. The single layer is 1.61 hours faster

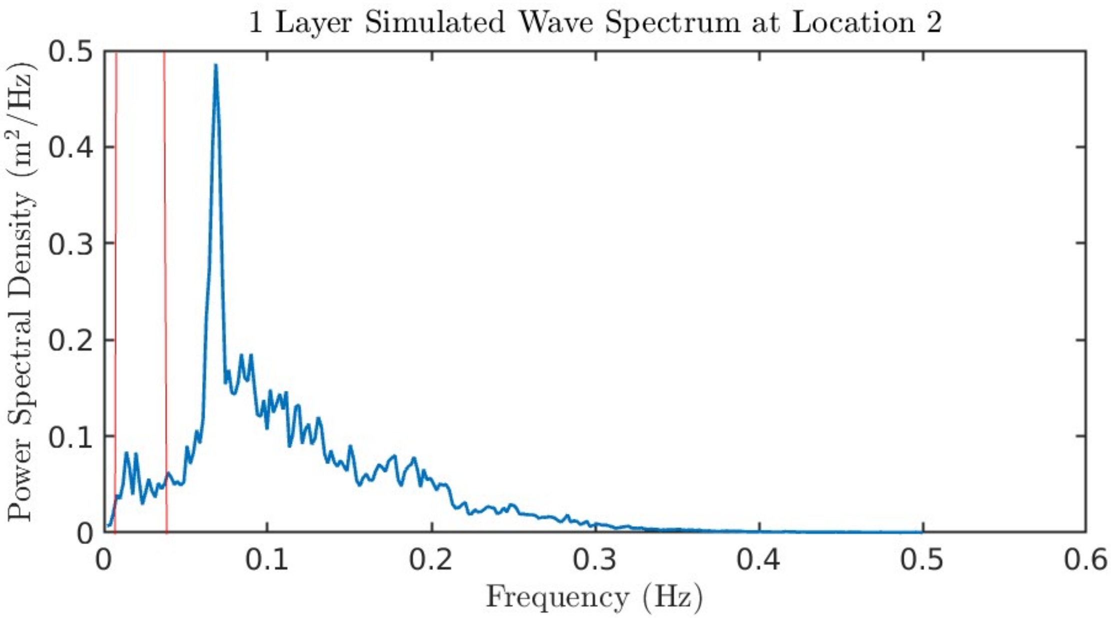

Figure 4.5 Simulated Wave Spectrum from 1 Layer Formulation at Location 2 (red lines indicate window of IG wave frequencies, where peak is 73.15 seconds)(Mannings n = 0.22)

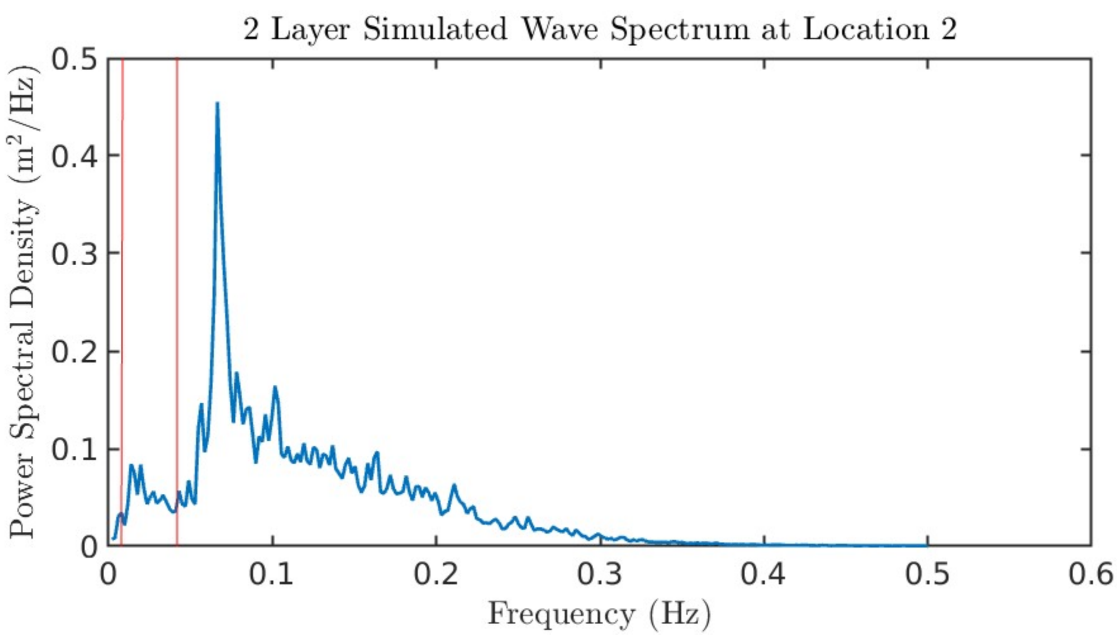

Figure 4.6 Simulated Wave Spectrum from 2 Layer Formulation at Location 2 (red lines indicate window of IG wave frequencies, where peak is 73.15 seconds)(Mannings n = 0.22)

	Simulation Time		File Size
	[seconds]	[hours]	[GB]
Single Layer	85242	23.68	101.1
Reduced Two-Layer	91709	25.47	105.1

Table 4.1 Simulation Characteristics for 1 and 2 Layer Simulations

than the two-layer and is 4 GB smaller. As memory has proven to be a limitation of the simulations (see Section 2.4.3), the smaller file size of the single layer would be preferable.

An additional point of interest in the model formulation study is the ratio between the two layers. Labeled as α in Figure 4.2, the ratio defines how the water column is divided. While this division may impact the simulation results, the optimization for α was not performed in this research. Furthermore, the single layer model is older and more extensively tested compared to newer or more complex version of the reduced two-layer model. Finally, Bai and Cheung (2016) found that the single layer formulation is valid up to a relative water depth (kh) of 1.2 and the reduced 2-layer formulation is valid up to a relative water depth of 3 (Bai and Cheung 2016). Given the input wave parameters have a kh of 0.86-1.11 at the offshore boundary depth, the single layer is still valid. For these reasons, the remaining simulation results were all prepared using the single layer formulation. Both model formulations have been shown to be suitable for the project site in this research.

4.4 Bottom Roughness Simulation Results

4.4.1 Mannings of 0.22

As described in Section 4.2, a Mannings n of 0.22 is suggested for the region of the project site where the pressure transducers were deployed. The domain used to study the single layer and reduced two-layer formulations included the coordinates at which the Location 2 pressure sensor was deployed. To explore the applicability of the Mannings coefficient at Location 3, an additional domain was set up to include its coordinates. The resolution of the grid and the user-defined spectral input that were used for the Location 2 domain

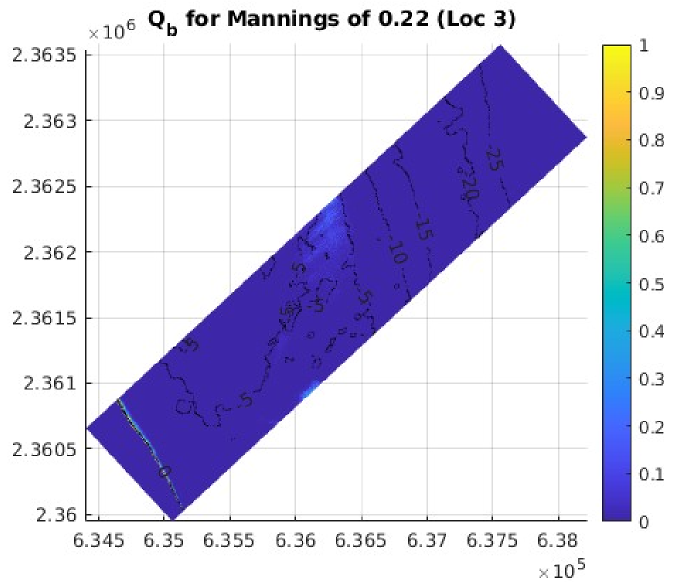

Figure 4.7 Probability of Breaking for Location 3 (Mannings n = 0.22)

remained the same for the second domain. The probability of breaking (Figure 4.7) at Location 3 displays a lower probability of breaking than at Location 2, which may be due to the difference in bathymetry. The spectra can be seen in Figure 4.8. The red lines show the minimum and maximum frequencies of IG waves. It is apparent both simulations were able to simulate IG waves, as there are peaks of the spectral density within the window.

Table 4.4.1 outlines the peak period, secondary period and IG wave period. Recall that the peak period found from PacIOOS wave buoy 098 was 14.55 seconds 4.2, 0.08 seconds less than the period found by both the simulation for Location 2 and for Location 3. The secondary peaks for both Location 2 and 3 are within 3.5 seconds of those found from the measured data. Comparing the IG waves from the measured data to the simulation, the peak periods have a difference of 31 seconds, or a 30% difference, at Location 2. At Location 3, there is a 39 second difference in frequencies, which could be attributed to nonlinear transfer of wave energy through three-wave and four-wave interactions in Equation 2.11. The nonlinear interactions contribute to the redistribution of energy across different frequencies within the wave spectrum, which may be reflected in these results.

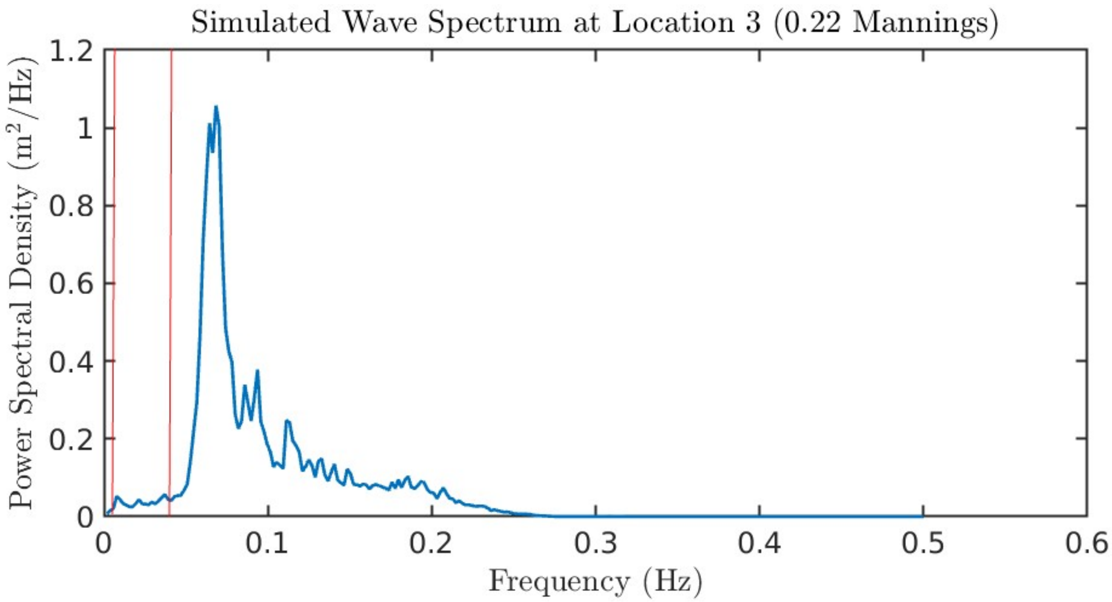

Figure 4.8 Simulated Wave Spectrum of Location 3 with Mannings of 0.22 (red lines indicate window of IG wave frequencies, where peak is 46.56 seconds)

	Peak Period (s)	Secondary Period (s)	IG Wave Period (s)
Location 2	14.63	11.91	71.32
Location 3	14.63	10.67	46.56

Table 4.2 Periods in Simulated Wave Spectra

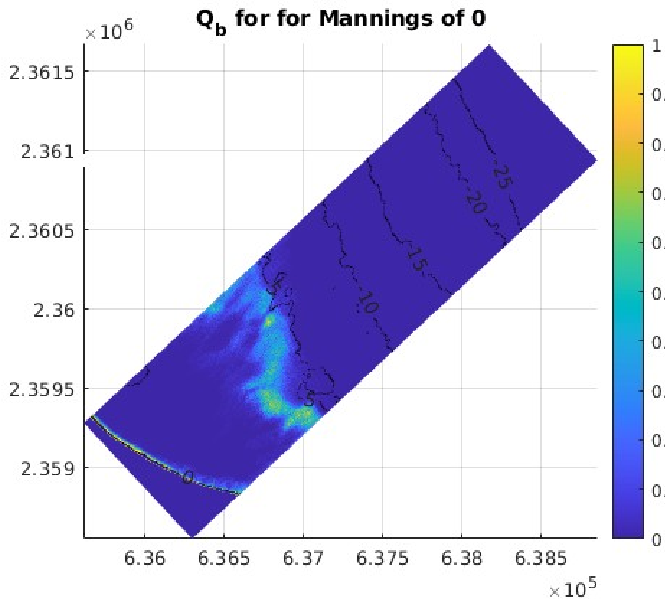

Figure 4.9 Probability of Breaking for Mannings of 0

	n = 0	n = 0.02	n = 0.11	n = 0.22
Peak IG period (s)	73.15	73.15	73.15	73.15
Peak IG PSD (m^2/Hz)	0.554	0.472	0.135	0.084

Table 4.3 IG Periods and Corresponding Power Spectral Density of Variable Mannings (n) Simulated Wave Spectra

4.5 Additional Bottom Roughness Simulation Results

To test how the presence of IG waves is impacted by bottom roughness and to better calibrate the simulation results with those of the field survey, additional Mannings coefficients were tested. As studies have shown that decreased bottom roughness will increase the presence of IG waves, three Mannings values of 0, 0.02 and 0.11 were selected as trial values (van Dongeren et al. 2012). The numerical scheme, such as grid resolution and offshore boundary, were kept the same as that implemented in the simulation which had a Mannings of 0.22. The map of probability of breaking can be seen in Figures 4.9, 4.10 and 4.11. The wave spectra calculated from each set of results at Location 2 can be seen in Figures 4.12, 4.13 and 4.14.

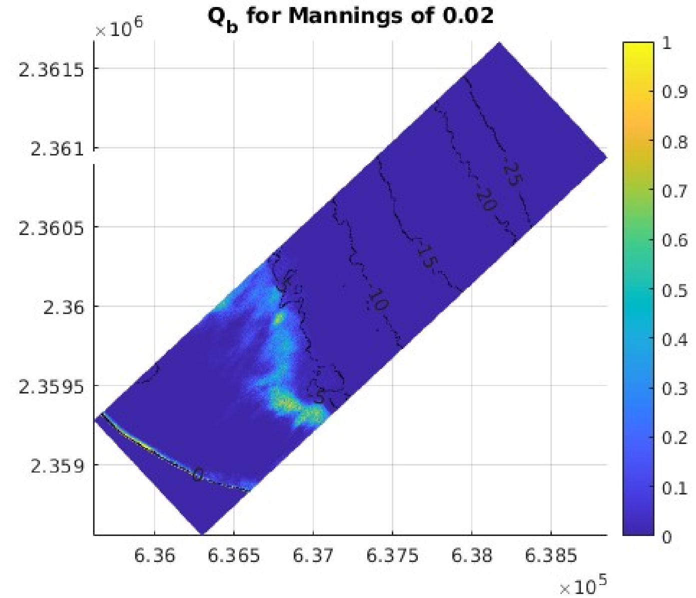

Figure 4.10 Probability of Breaking for Mannings of 0.02

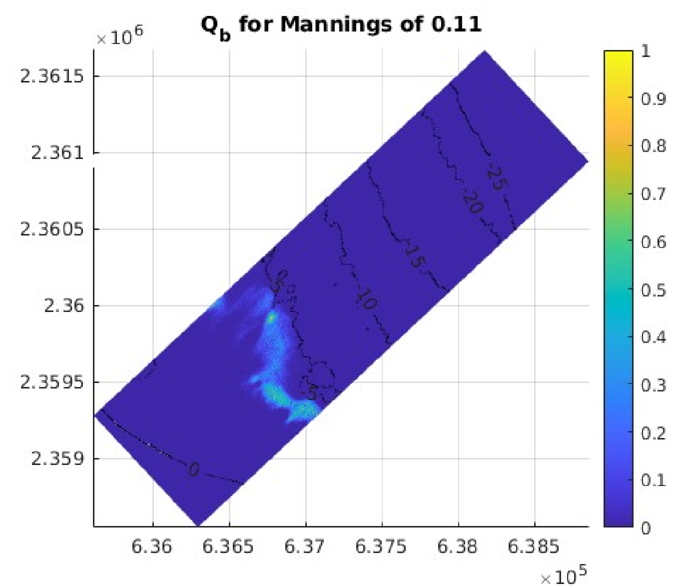

Figure 4.11 Probability of Breaking for Mannings of 0.11

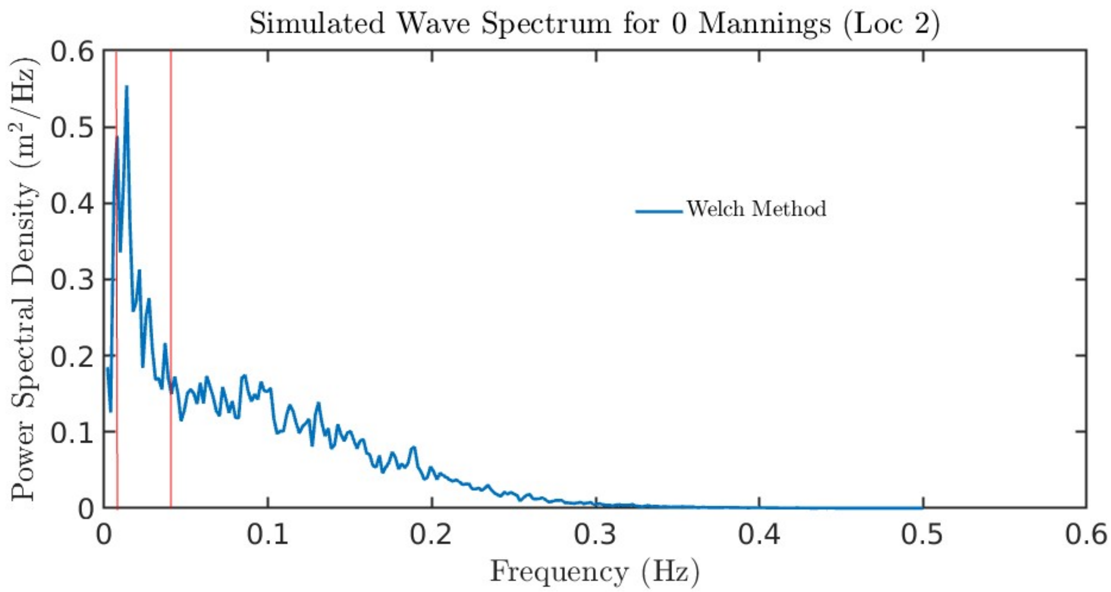

Figure 4.12 Simulated Wave Spectrum of Location 2 with Mannings of 0 (red lines indicate window of IG wave frequencies, where peak is 73.15 seconds)

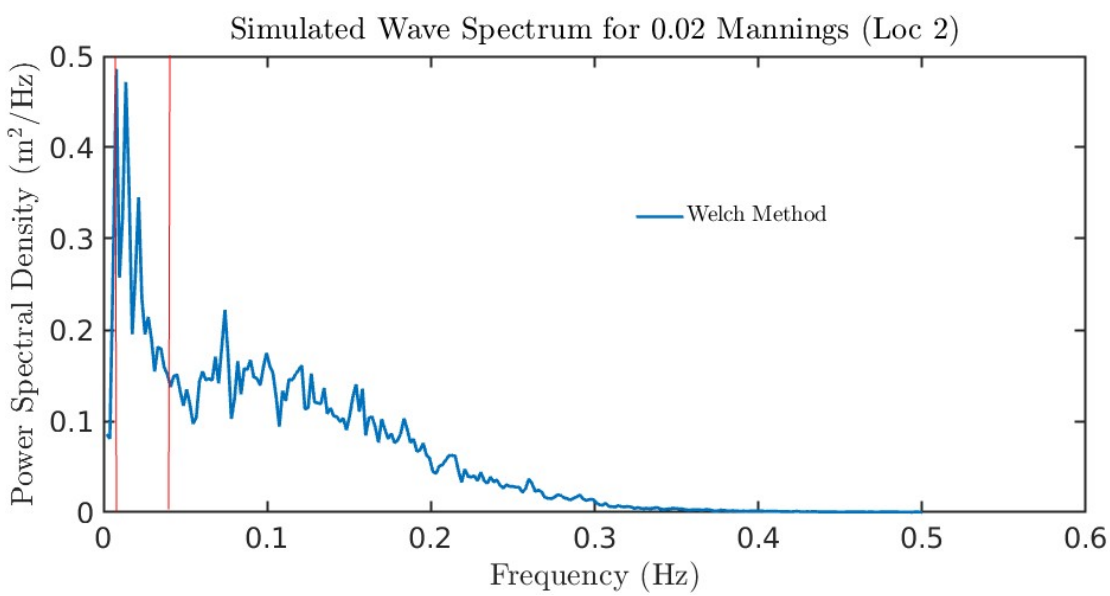

Figure 4.13 Simulated Wave Spectrum of Location 2 with Mannings of 0.02 (red lines indicate window of IG wave frequencies, where peak is 73.15 seconds)

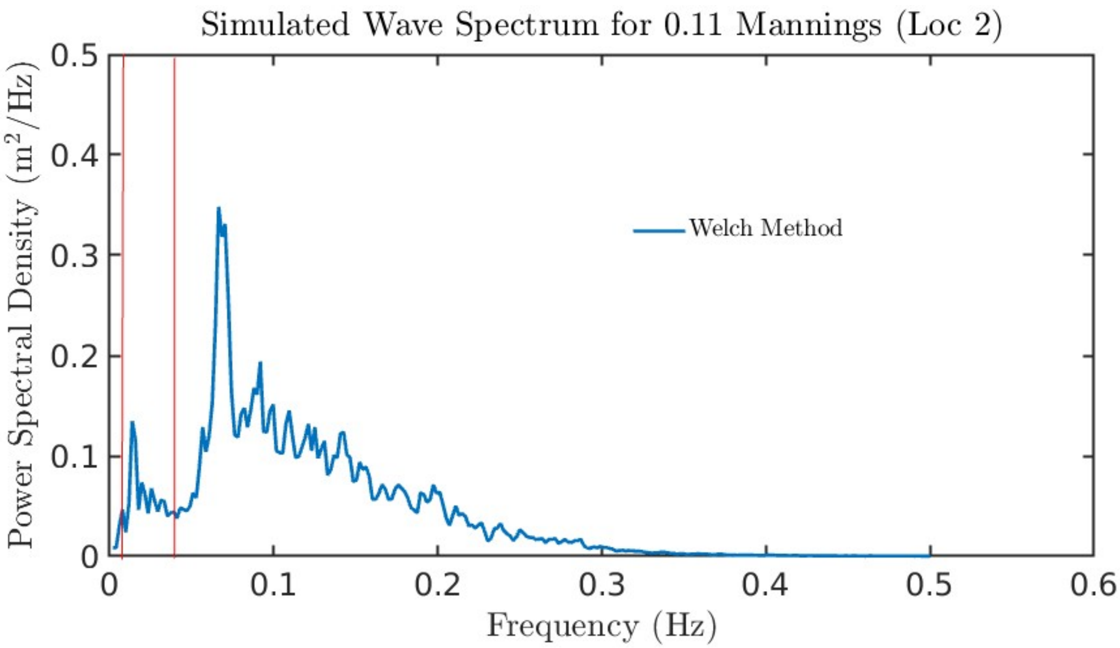

Figure 4.14 Simulated Wave Spectrum of Location 2 with Mannings of 0.11 (red lines indicate window of IG wave frequencies, where peak is 73.15 seconds)

Comparing the probability of breaking for the ranging Mannings coefficients, the overall probability is increased as the value decreases. As bottom roughness acts to dissipate wave energy, a lower bottom friction would give a higher probability of breaking. Though the Q_b values are relatively close between 0.11 and 0.22, the trend is still applicable. Furthermore, the difference in energy distribution reflected in Q_b maps is seen in the calculated spectra. Literature has found that increased bottom roughness results in a decreased presence of IG waves (Lowe et al. 2005). Table 4.5 summarizes the IG wave characteristics for each Mannings value. While the period of the IG waves remains constant between the different Mannings coefficients (73.15 seconds), the magnitude of the power spectral density does not. The magnitude found using a Mannings of 0 is 6.5 times greater than the magnitude found using a Mannings of 0.22, suggesting that increased bottom roughness decreases the IG wave presence.

Comparing the simulated results to the field survey spectrum, the Mannings coefficient of 0.11 seems to best match at Location 2. The power spectral density at the peak period

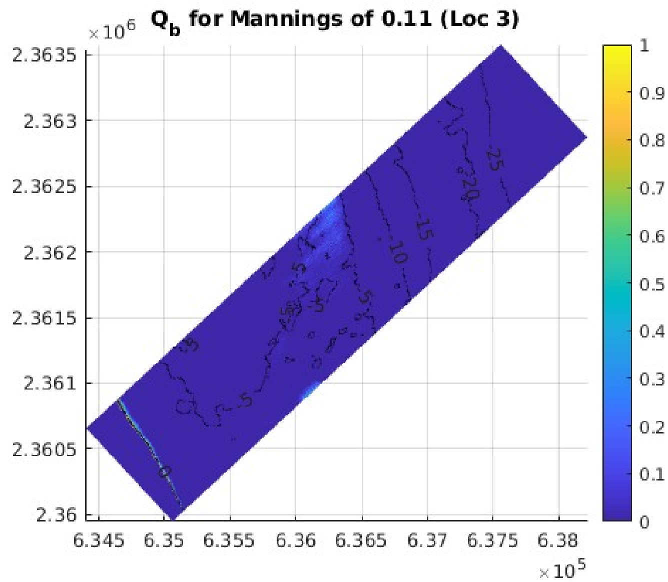

Figure 4.15 Probability of Breaking for Mannings of 0.11 at Location 3

(12.80 seconds) of the field results is 0.361 m^2/Hz. In comparison, the power spectral density at the peak period (14.22 seconds) for the Mannings of 0.11 is 0.348 m^2/Hz, which is the closest in magnitude out of the simulation results.

As the Mannings of 0.11 seemed to be the best fit, it was implemented at Location 3. Figure 4.15 shows the map of the probability of breaking and Figure 4.16 shows the calculated spectrum based on the simulation results. The probability of breaking for the Mannings value of 0.11 is increased in comparison to the probability when a 0.22 Mannings value is used. This aligns with the results at Location 2, where the probability of breaking decreases as the bottom roughness increases. The spectrum calculated using the 0.11 Mannings value has a higher power spectral density at the peak period in comparison to the 0.22 Mannings value. The magnitude of the IG waves is also increased. Comparing both bottom roughness values to the field observations, 0.22 aligns more closely. This may suggest multiple Mannings values should be applied to a given domain.

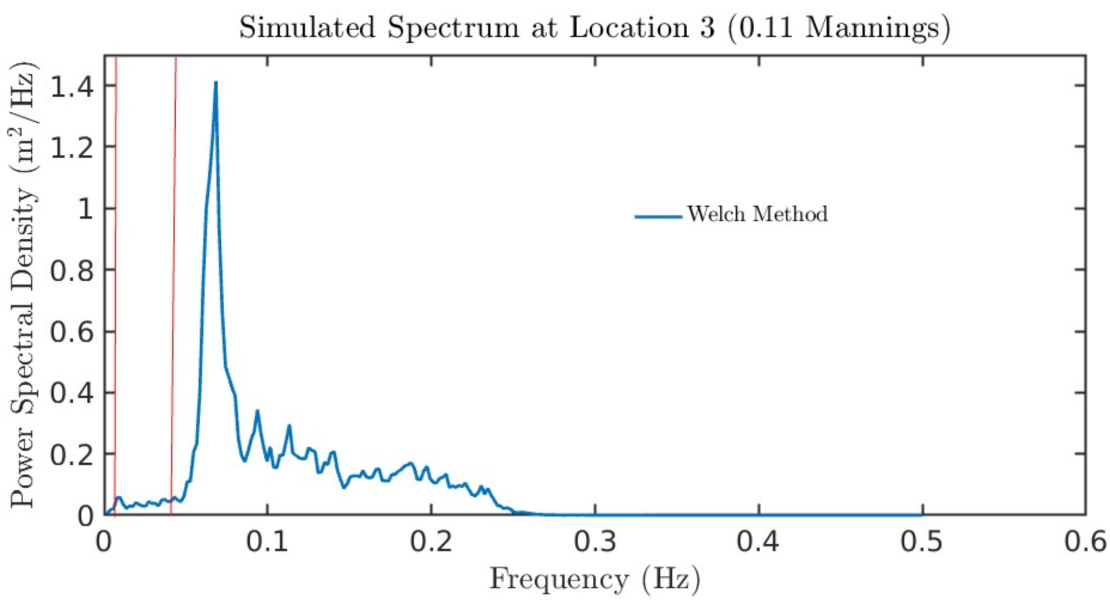

Figure 4.16 Simulated Wave Spectrum of Location 3 with Mannings of 0.11 (red lines indicate window of IG wave frequencies, where peak is 46.56 seconds)

Chapter 5

Conclusions and Recommendations for Future Work

5.1 Conclusions

This study utilized the nonhydrostatic version of XBeach to simulate wave transformations in a nearshore environment. The fundamental hypotheses to be tested in this research are as follows:

1. The nonhXB model can be effectively implemented to study the wave transformations of a fringing reef.

2. The field data collected using pressure sensors can be used to calibrate and verify the nonhXB model results.

3. NonhXB is capable of simulating infragravity (IG) waves for the project location.

4. Bottom roughness has a significant impact on the simulation results, in particular, the IG waves.

The answers to these hypotheses are investigated by analyzing the data collected during the field survey at Waimānalo Beach, as well as a numerical study of the wave transformations using nonhydrostatic XBeach.

Chapter 2 outlined the numerical setup and gave details on how the model is implemented. It described a one-way coupling method between SWAN, an additional model that provides the offshore boundary, and nonhXB, as well as how the domain and grid of the simulations are set up. The method of calculating the probability of wave breaking was defined both in terms of the nonhXB model and post-processing using the zero-crossing method. Furthermore, the methodology of performing a spectral analysis and calculating power was outlined. Finally, the procedure to analyze and convert the field observations and buoy data into comparable data was provided.

Chapter 3 covered the field observations that were made at Waimānalo Beach. The field study took place on October 20, 2023 and was conducted to be compared to nonhXB numerical simulation results as validation and calibration. Three locations were selected along the beach and four pressure transducers were deployed in the water. Though only two were able to be recovered, both locations provided a reasonable time series and wave spectrum. An additional data point was collected from pacIOOS buoy 098 on the day of the field survey and was found to be in relative accordance with the pressure transducer results. A slight error occurred, which may be due to physical processes not studied in this project, such as nonlinear wave interactions and the current. IG waves were found in the spectra of both locations.

Chapter 4 included the simulation results that aim to answer the four hypotheses. To improve the performance of the model, a user-defined spectral input was implemented at the offshore boundary. The input was taken from the time series at buoy 098 in an effort to improve accuracy. A Mannings coefficient of 0.22 was used as a starting value for the numerical scheme, as was suggested by a prior study that was conducted at the project site. The two common model formulations (single layer and reduced two-layer) were tested for suitability for this project site. It was concluded that both models produce a reasonable agreement with the field results, however the single layer was selected due to computational expense, simplicity and more extensive testing.

Chapter 4 additionally studied how the Mannings coefficient may impact the simulation results. The suggested Manning's value of 0.22 was implemented at both Location 2 and Location 3. The results showed a reasonable comparison with the field observation results, including the peak period and IG waves. To explore the impact of changing the bottom roughness on the results, additional Mannings coefficients of 0, 0.02 and 0.11 were tested. It was shown that bottom roughness does has a significant impact on the simulation results, especially the IG waves. The probability of wave breaking increased as the bottom roughness decreased, which was reflected in the wave spectra. The magnitude of the IG waves was reduced as the bottom roughness increased, as well as the magnitude of the peak period. Furthermore, it was found that a Mannings value of 0.11 best aligned with the results of the field survey at Location 2, while 0.22 best aligned with the field observations at Location 3. The peak period and IG waves were accurately modeled, concluding that nonhXB can be effectively implemented to study the wave transformations of the fringing reef at Waimānalo Beach.

5.2 Recommendations for Future Work

Although this research concluded the field observations and nonhXB simulation results are within reasonable agreement of each other, there are several aspects that could be improved. One key recommendation is to deploy additional pressure sensors across the study area to obtain a more complete understanding of the in-situ wave conditions. Deploying pressure sensors at variable depths along the fringing reef would allow for an increased understanding of the IG waves across the reef flat, as well as how the wave energy is transformed towards the shore. Additionally, collecting site characteristics, such as the dimensions of the coral reef where the pressure transducers are deployed, could provide a better calibration for the simulations. Mapping the bottom roughness could allow for more accurate results, as it has been proven to have a significant impact on the model.

As discussed in the first chapter, the original plan of this research was to conduct a full field survey at Fort Hase Beach. This study included taking video footage from a vantage point to better quantify the probability of breaking. Though using a drone would be optimal, permitting regulations on American military bases prohibit the use of drones. Drone footage would allow for calibration and comparison with the Q_b calculated from numerical simulation results, highlighting any discrepancies. It could also be used to study runup and flooding at the beach, parameters out of the scope of this thesis but affected by wave transformations, especially bottom roughness.

In terms of the numerical scheme, the implementation of a variable grid could allow for a more efficient model. Finer grid resolutions require higher computational expenses but are not always necessary for the entirety of the domain. Increasing the resolution in the area of most interest, for example, the breaker zone, but maintaining a slightly larger resolution in other areas could be a method of achieving more accurate results without sacrificing computation time.

Finally, edge waves were described in Chapter 1 as IG waves that have been trapped along the shore. While they were not studied in this project, it is important to understand whether the IG waves that were observed were driven by edge waves. To determine the presence of edge waves, the breaker zone dynamics and natural frequency can be used. A primary generation mechanism for IG waves is wave breaking. By studying the oscillations in the breaker zone, the frequency can be compared to the observation conditions of the IG waves from the pressure transducers. If the two align, the oscillations are likely due to IG waves. Furthermore, there is a relationship between the distance between the two headlands and the natural frequency that occurs. If the frequency aligns with the observed conditions, edge waves may be present. It would be recommended to conduct these two methods to determine if there is a presence of edge waves.

Appendix A

Waimānalo Beach Field Study Details

A.1 Field Deployment

The field survey at Waimānalo Beach took place on October 20, 2023. It was used as a substitution for a field survey at Fort Hase beach, which did not occur due its lack of accessibility and dangerous wave conditions. The field observations were used as a method of validating the nonhXB simulations that were ran at the same site. The results were discussed in Chapter 4, however the details of the study itself are outlined below.

The project has access to 10 U20 HOBOWare pressure sensors to measure the water surface elevation in the field. The pressure transducers were deployed for 4 hours in the water, while one remained on shore to measure the barometric pressure for a baseline. As impact with hard surfaces may damage the sensors and cause errors in the readings, a housing was fabricated from plastic pencil cases and zip ties. Dive weights were zip-tied to the interior of the case to ensure stability and that the sensors remain submerged, while the pressure sensors were be zip-tied on the top of the case.

A team of at least 2 free divers, 2 support personnel and 1 person were to remain on shore was required for the surveys. The following materials were required:

- Water vessel
- U20 HOBOWare Pressure Transducers

- Zip Ties
- Plastic pencil cases
- Shoreline Marine Boat Fenders
- Shoreline Marine Multi Purpose Braid Nylon
- Cinder blocks
- Dive Weights
- Garmin Marine GPS
- GoPro Camera
- On-shore camera

The sensors were set up using the HOBOWare software to read data for 6 hours at 1 Hz. They were calibrated using a bucket of water prior to deployment. The housed sensors were tied to a cinder block as an anchor and boat fenders acted as surface buoys to locate where the submerged sensors are located. The team deployed a vessel to reach the deployment locations and the free divers placed the cinder block on the seafloor and attached the sensor. All the pressure sensors were placed in succession. The sensors were deployed by the free divers, one team member remained in the kayak for controlled operation. Data was collected for 4 hours, before being recovered by the free divers and returned to shore.

As discussed in Chapter 4, the two sensors placed at Location 4 were not able to be recovered. Because the sensors were not attached to the mooring buoys and were placed in relatively shallow, high-energy water, both sensors were displaced at a distance too far from the buoy for the divers to locate. It is recommended to attach the sensors to the mooring line with shoreline marine nylon rope using ample slack to avoid additional loss of equipment for future field observations.

Furthermore, the locations at which the sensors were deployed were not the intended locations that were decided when planning the survey. The span between the different original locations was around a mile and a half; kayaking and free diving proved to be physically strenuous, causing the team to shorten the distance between the deployment locations. Location 4 was observed to have an increased undertow than the intended location, contributing to the missing sensors. A motorized boat or more strategic pressure sensor drop sites would be recommended for future fieldwork.

A.2 Data

This section outlines the raw data collected by the wave buoy and pressure transducers. Figure A.1 displays the format of the data provided by CDIP for PacIOOS buoy 098. Column 1 is the sample time in UTC. Column 2 and 3 show the displacement in the North/South direction and West/East direction in meter. These were not implemented for this project. Next, column 4 shows the vertical displacement in meters of the buoy. The vertical displacement is the variable used to represent the water surface elevation for the time series calculated in Chapter 3. The final column is the flag, which marks how CDIP stores the dataset.

Sample time(UTC)	N/S(m)	W/E(m)	Vert(m)	Flag
20231020000000.03125	0.800	0.670	0.750	2
20231020000000.81250	0.230	0.620	0.990	2
20231020000001.59375	-0.200	0.220	1.080	2
20231020000002.37500	-0.720	-0.110	0.900	2

Figure A.1 Raw Buoy Data from PacIOOS 098

The raw data collected from the HOBOware sensors at Location 2 and 3 can be seen in Figures A.2 and A.3. Location 2 shows a slightly downward trend in the absolute pressure (shown in black). This trend is not observed in Figure A.3 at Location 3. This is likely due to the difference in water depth. Location 2 is at a depth of 2.5 meters while Location 3 is at a depth of 8 meters. The temperature is observed to increase over time at Location 2, impacting the density of the seawater. An increase in temperature results in a decreased seawater density. Referring to Equation 2.14, decreasing the density will result in a decreased pressure. The deeper location of Location 3 does not display this, as deeper water displays a slower change in temperature. This may be producing the zero frequency component seen in the calculated wave spectrum at Location 2.

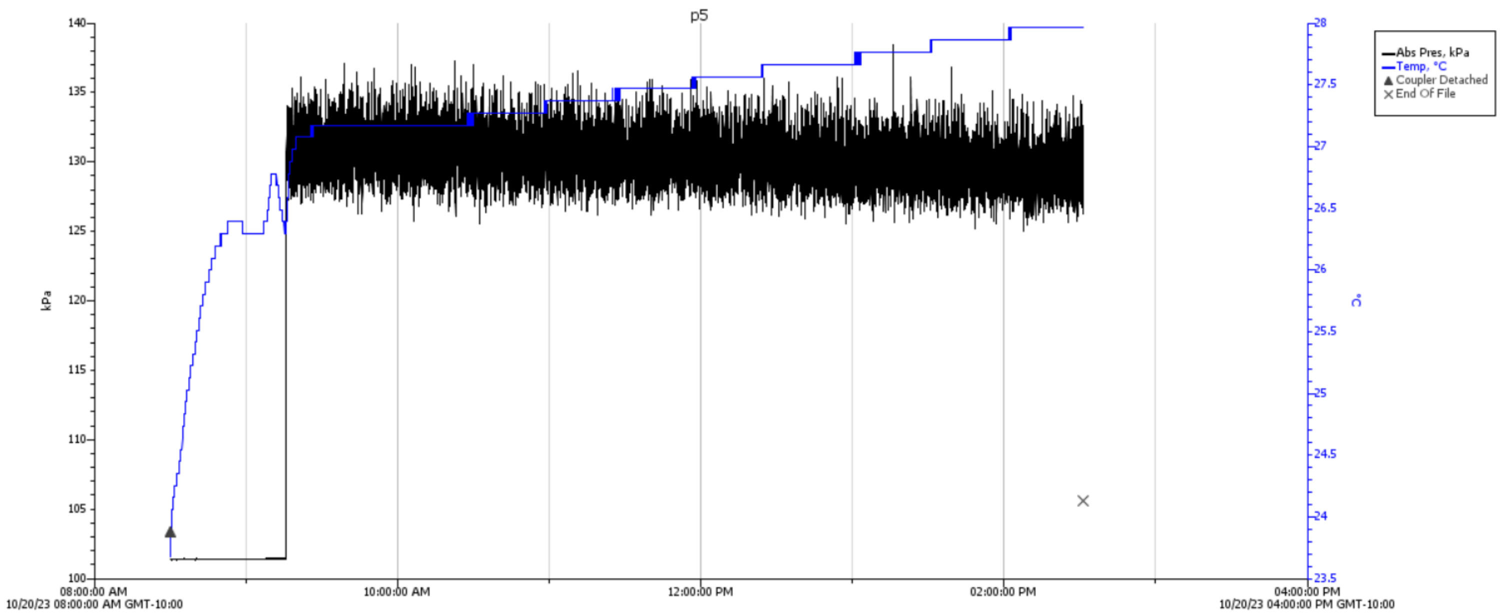

Figure A.2 Raw HOBOware Pressure Sensor Data at Location 2

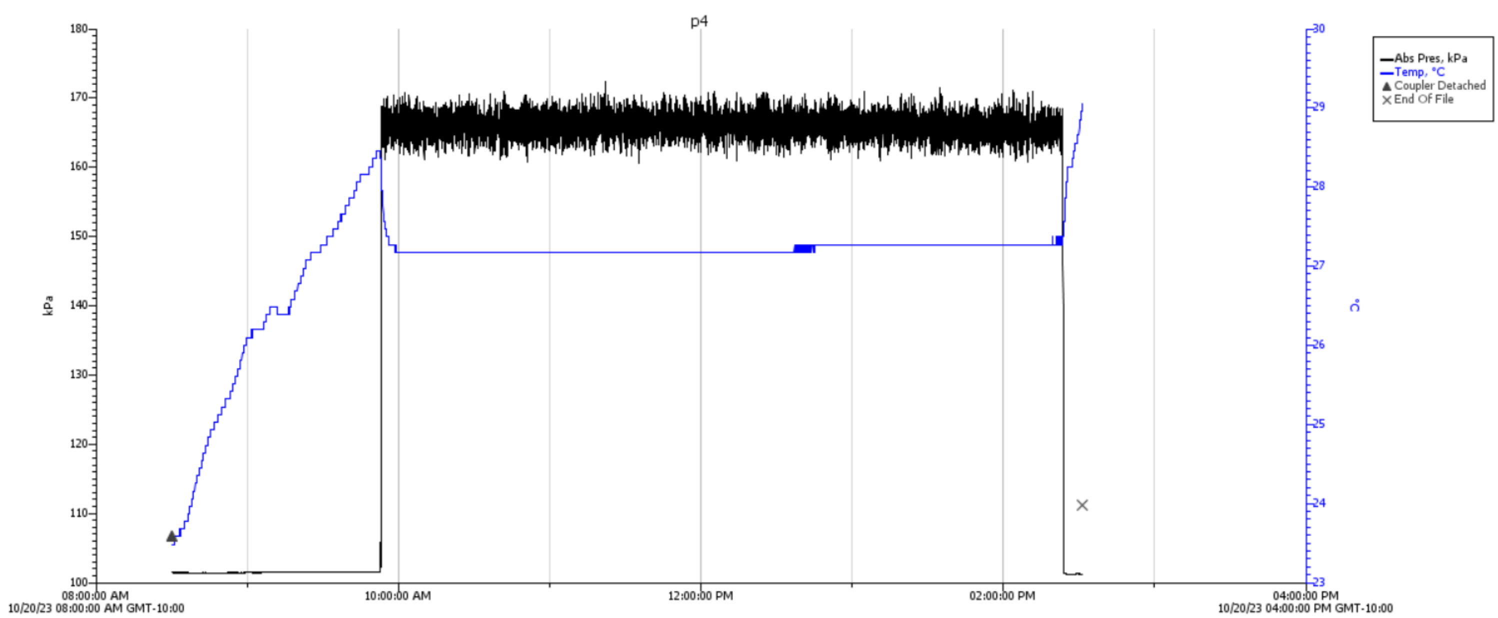

Figure A.3 Raw HOBOware Pressure Sensor Data at Location 3

References

Bai, Y. and Cheung, K. F. (2016). Linear and nonlinear properties of reduced two-layer models for non-hydrostatic free-surface flow. *Ocean Modelling*, 107:64–81.

Bertin, X., de Bakker, A., van Dongeren, A., Coco, G., André, G., Ardhuin, F., Bonneton, P., Bouchette, F., Castelle, B., Crawford, W. C., Davidson, M., Deen, M., Dodet, G., Guérin, T., Inch, K., Leckler, F., McCall, R., Muller, H., Olabarrieta, M., Roelvink, D., Ruessink, G., Sous, D., Éléonore Stutzmann, and Tissier, M. (2018). Infragravity waves: From driving mechanisms to impacts. *Earth-Science Reviews*, 177:774–799.

Booij, N., Ris, R. C., and Holthuijsen, L. H. (1999). A third-generation wave model for coastal regions: 1. model description and validation. *Journal of Geophysical Research: Oceans*, 104(C4):7649–7666.

Buckley, M., Lowe, R., and Hansen, J. (2014). Evaluation of nearshore wave models in steep reef environments. *Ocean Dynamics*, 64:847–862.

Buckley, M., Lowe, R., Hansen, J., Dongeren, A., Pomeroy, A., Storlazzi, C., Rijnsdorp, D., F. da Silva, R., Contardo, S., and Green, R. (2022). Wave-driven hydrodynamic processes over fringing reefs with varying slopes, depths, and roughness: Implications for coastal protection. *Journal of Geophysical Research: Oceans*, 127.

Buckley, M. L., Lowe, R. J., Hansen, J. E., and Dongeren, A. R. V. (2016). Wave setup over a fringing reef with large bottom roughness. *Journal of Physical Oceanography*, 46(8):2317 – 2333.

Chase, J. (2023). Using nonhydrostatic xbeach to simulate wave transformations in fringing reef environments.

Cheung, K. F., Phadke, A., Wei, Y., Rojas, R., Douyere, Y.-M., Martino, C., Houston, S., Liu , P., Lynett, P., Dodd, N., Liao, S., and Nakazaki, E. (2003). Modeling of storm-induced coastal flooding for emergency management. *Ocean Engineering*, pages 1353–1386.

Cialone, M. and Smith, J. (2007). Wave transformation modeling with bottom friction applied to southern oahu reefs. *10th International Workshop on Wave Hindcasting and Forecasting Coastal Hazard Assessment*.

de Ridder, M. P., Smit, P. B., van Dongeren, A. R., McCall, R. T., Nederhoff, K., and Reniers, A. J. (2021). Efficient two-layer non-hydrostatic wave model with accurate dispersive behaviour. *Coastal Engineering*, 164:103808.

Fletcher, C., Romine, B., Genz, A., Barbee, M., Dyer, M., Anderson, T., Lim, S., Vitousek, S., Bochicchio, C., and Richmond, B. (2012). National assessment of shoreline change: Historical shoreline change in the hawaiian islands.

Hasselmann, K., Barnett, T., Bouws, E., Carlson, H., Cartwright, D., Enke, K., Ewing, J., Gienapp, H., Hasselmann, D., Kruseman, P., Meerburg, A., Muller, P., Olbers, D., Richter, K., Sell, W., and Walden, H. (1973). Measurements of wind-wave growth and swell decay during the joint north sea wave project (jonswap). *Deut. Hydrogr. Z.*, 8:1–95.

Huntley, D. A. and Bowen, A. J. (1973). Field observations of edge waves. *Nature*, 243:160–162.

Jacobs, R. P. M. (2010). Non-hydrostatic computations of nearshore hydrodynamics. *TU Delft*.

Johnson, R. S. (2007). Edge waves: Theories past and present. *Philosophical Transactions: Mathematical, Physical and Engineering Sciences*, 365(1858):2359–2376.

Komen, G. J., Cavaleri, L., Donelan, M., Hasselmann, K., Hasselmann, S., and Janssen, P. A. E. M. (1994). Dynamics and modelling of ocean waves.

Lashley, C. H., Roelvink, D., van Dongeren, A., Buckley, M. L., and Lowe, R. J. (2018). Nonhydrostatic and surfbeat model predictions of extreme wave run-up in fringing reef environments. *Coastal Engineering*, 137:11–27.

Lowe, R., Falter, J., Bandet, M., Pawlak, G., Atkinson, M., Monismith, S., and Koseff, J. (2005). Spectral wave dissipation over a barrier reef. j geophys res 110(c4), c04001. *J. Geophys. Res*, 110.

McCall, R., Masselink, G., Poate, T., Roelvink, J., and Almeida, L. (2015). Modelling the morphodynamics of gravel beaches during storms with xbeach-g. *Coastal Engineering*, 103:52–66.

McCall, R., Masselink, G., Poate, T., Roelvink, J., Almeida, L., Davidson, M., and Russell, P. (2014). Modelling storm hydrodynamics on gravel beaches with xbeach-g. *Coastal Engineering*, 91:231–250.

McCall, R., Roelvink, D., van Dongeren, A., Quataert, E., de Bakker, A., de Ridder, M., de Goede, R., de Vet, L., and van der Lugt, M. (2022). *XBeach Documentation*. Release BOI-phase3-5956.

Mei, C. (1983). *The applied dynamics of ocean surface waves*. Wiley.

Nielsen, P. (1992). *Coastal Bottom Boundary Layers and Sediment Transport*. World Scientific Publishing, Singapore, Singapore.

Rijn, L. C. V. (1993). *Principles of Sediment Transport in Rivers, Estuaries, and Coastal Seas*. Aqua Publications, Amsterdam.

Rossi, G. B., Crenna, F., Piscopo, V., and Scamardella, A. (2020). Comparison of spectrum estimation methods for the accurate evaluation of sea state parameters. *Sensors*, 20(5).

Selman, M. (2023). Analysis of xbeach non-hydrostatic model capability in processing swan spectral input.

Sheremet, A., Kaihatu, J., Su, S.-F., Smith, E., and Smith, J. (2011). Modeling of nonlinear wave propagation over fringing reefs. *Coastal Engineering*, 58(12):1125–1137.

Smagorinsky, J. (1963). General circulation experiments with the primitive equations: I. the basic experiment. *Monthly Weather Review*, 91(3):99 – 164.

Smit, P., Stelling, G., Roelvink, D. J., Thiel de Vries, J., McCall, R., van Dongeren, A., Zwinkels, C., and Jacobs, R. (2010). Xbeach: Non-hydrostatic model: Validation, verification and model description.

Stelling, G. and Zijlema, M. (2003a). An accurate and efficient finite-difference algorithm for non-hydrostatic free-surface flow with application to wave propagation. *International Journal for Numerical Methods in Fluids*, 43(1):1–23.

Stelling, G. and Zijlema, M. (2003b). An accurate and efficient finite-difference algorithm for non-hydrostatic free-surface flow with application to wave propagation. *International Journal for Numerical Methods in Fluids*, 43:1 – 23.

Stopa, J., Filipot, J.-F., Li, N., Cheung, K. F., Chen, Y.-L., and Vega, L. (2013). Wave energy resources along the hawaiian island chain. *Renewable Energy*, 55:305–321.

SWAN-Team (2006). User manual swan cycle iii version 41.45ab.

Vaidyanathan, P. (2001). Generalizations of the sampling theorem: Seven decades after nyquist. *IEEE Transactions on Circuits and Systems I: Fundamental Theory and Applications*, 48(9):1094–1109.

van Dongeren, A., Lowe, R., Pomeroy, A., Duong, T., Roelvink, D. J., Symonds, G., and Ranasinghe, R. (2012). Modelling infragravity waves and currents across a fringing coral reef. volume 1.

Zijlema, M. and Stelling, G. (2008). Efficient computation of surf zone waves using the nonlinear shallow water equations with non-hydrostatic pressure. *Coastal Engineering*, 55(10):780–790.